JGR Atmospheres

RESEARCH ARTICLE
10.1029/2019JD030831

Characteristics of Ice Nucleating Particles in and Around California Winter Storms

Ezra J.T. Levin[1], Paul J. DeMott[1], Kaitlyn J. Suski[1,2], Yvonne Boose[3], Thomas C.J. Hill[1], Christina S. McCluskey[4], Gregory P. Schill[5], Katherine Rocci[1], Hashim Al-Mashat[6], Louise J. Kristensen[6], Gavin Cornwell[6], Kimberly Prather[6], Jason Tomlinson[7], Fan Mei[7], John Hubbe[7], Mikhail Pekour[7], Ryan Sullivan[8], L. Ruby Leung[7], and Sonia M. Kreidenweis[1]

[1]Colorado State University, Fort Collins, CO, USA, [2]Now at JUUL Labs, San Francisco, CA, USA, [3]Deutsches Zentrum fur Luft- und Raumfahrt, Oberpfaffenhofen, Germany, [4]NCAR, Boulder, CO, USA, [5]NOAA ESRL, Boulder, CO, USA, [6]Department of Chemistry and Biochemistry, University of California, San Diego, La Jolla, CA, USA, [7]PNNL, Richland, WA, USA, [8]Department of Chemistry, Carnegie Mellon University, Pittsburgh, PA, USA

Key Points:
- Ice nucleating particle number concentrations varied by a factor of 100 or more during a wintertime coastal California aircraft campaign
- Ice nucleating particle number concentrations in the airmass associated with an atmospheric river were less than 1 per liter at −25 °C
- Marine aerosol were the likely dominate source of ice nucleating particles for the atmospheric river event

Correspondence to:
E. J. T. Levin,
elevin@atmos.colostate.edu

Citation:
Levin, E. J. T., DeMott, P. J., Suski, K. J., Boose, Y., Hill, T. C. J., McCluskey, C. S., et al. (2019). Characteristics of ice nucleating particles in and around California winter storms. *Journal of Geophysical Research: Atmospheres*, *124*, 11,530–11,551. https://doi.org/10.1029/2019JD030831

Received 15 APR 2019
Accepted 15 SEP 2019
Accepted article online 12 OCT 2019
Published online 14 NOV 2019

©2019. American Geophysical Union. All Rights Reserved.

Abstract A major component of California's yearly precipitation comes from wintertime atmospheric river events which bring large amounts of moisture from the tropics up to the midlatitudes. Understanding these systems, specifically the effects of aerosol particles on precipitation associated with these storms, was a major focus of the 2015 Atmospheric Radiation Measurement Cloud Aerosol Precipitation Experiment, which was part of the wintertime California Water 2015 campaign. The measurement campaign provided sampling platforms on four aircraft, including the Atmospheric Radiation Measurement Aerial Facility G-1, as well as the National Oceanic and Atmospheric Administration Ronald H. Brown research vessel and at a ground station in Bodega Bay, CA. Measurements of ice nucleating particles (INPs) were made with the Colorado State University Continuous Flow Diffusion Chamber aboard the G-1, and aerosol filters were collected on the G-1, at the Bodega Bay site and on the Ronald H. Brown for postprocessing via immersion freezing in the Colorado State University Ice Spectrometer. Aerosol composition was measured aboard the G-1 with the Aerosol Time-of-Flight Mass Spectrometer. Here we present INP concentrations and aerosol chemical compositions during the course of the aircraft campaign. During the atmospheric river event, we found that marine aerosol was the main aerosol type and that marine INPs were dominant at cloud activation temperatures, which is in stark contrast to the dominance of dust INPs during the atmospheric river events in the California Water 2011 campaign.

1. Introduction

A large fraction of California's yearly precipitation comes from atmospheric river (AR) events, long thin bands of enhanced water vapor transport stretching from the tropics up into the midlatitudes. While AR events are a vital source of water for the western United States (Kim et al., 2018), with storms associated with these events estimated to provide 30–50% of the total precipitation to this region (Dettinger et al., 2011), ARs are also often associated with extreme precipitation and flooding (Dettinger et al., 2011). For example, from 2012–2016 most of California was under severe drought conditions with half of the state being classified as experiencing exceptional drought (Ralph et al., 2016; Swain et al., 2018). In 2017, heavy rain associated with increased AR activity ended the drought in much of the state. However, the storms brought so much precipitation that some regions were flooded, leading to extensive damage to roadways and dams, such as the Orville Dam which came close to failure (Swain et al., 2018). Events like these, both the multiyear drought and subsequent flooding, highlight the importance of understanding the controlling mechanisms for precipitation in this region and improving our ability to forecast changes to these mechanisms. While the availability of condensable water vapor is crucial to the intense rain and snow events associated with ARs (Ralph et al., 2013), the role of aerosol particles, especially those capable of initiating ice crystal formation, is less well understood and has been the focus of recent study (Ault et al., 2011; Creamean et al., 2013; Creamean et al., 2015; Fan et al., 2014; Fan et al., 2017; Martin et al., 2019; Rosenfeld et al., 2013).

Heterogeneous ice nucleation in mixed-phase clouds is an important process controlling the timing and amount of precipitation as well as cloud lifetime and brightness, which are also important for radiative balance (DeMott et al., 2010). In the absence of ice nucleating particles (INPs), liquid water drops must cool to

around −38 °C before freezing homogeneously (Vali et al., 2015). With an INP, however, supercooled liquid droplets can freeze at warmer temperatures, depending on the type and surface characteristics of the nucleating particle (DeMott et al., 2010; Hoose & Moehler, 2012). Through secondary ice formation processes, such as rime-splintering following the growth of single crystals (Hallett & Mossop, 1974) or various shattering/bursting processes that can occur at the point of freezing of drizzle-sized and larger supercooled droplets (Lauber et al., 2018), the effects of the initial INP on cloud and precipitation properties may be amplified. Therefore, the presence or absence of INPs in clouds can greatly influence glaciation, riming, and other processes which directly affect the formation, timing, and amount of precipitation. Despite their importance, INPs are relatively rare in the atmosphere with typical concentrations of only 1–10 per liter of air active at −30 °C in the free troposphere (Lacher et al., 2018). The type of INP present in a cloud can also greatly impact the temperature at which cloud droplets freeze or ice crystals form. Mineral dust particles may initiate freezing over a range of temperatures but are most efficient below −20 °C, while some biological organisms can cause droplets to freeze at temperatures as warm as −5 °C (Murray et al., 2012). Given their low abundance and the large range in temperatures over which different INP types can initiate ice crystal formation, there is still considerable uncertainty in how INPs affect cloud formation, leading to large uncertainties in modeling of mixed-phase and ice clouds and the resulting precipitation from these clouds (Fan et al., 2017).

Specifically, in the case of orographic precipitation associated with landfalling AR events in California, one suggested mechanism for the role of INPs in affecting precipitation totals is through the "seeder feeder" mechanism (Choularton & Perry, 1986; Creamean et al., 2014). In this proposed mechanism, ice crystals form in the upper layers of orographic clouds and then fall though a supercooled liquid layer, collecting rime and growing much larger before reaching the ground. This mechanism requires the presence of INPs at higher altitudes in the cloud, with the number and type of INPs greatly impacting the timing and amount of ice crystal formation. Riming efficiency, and thus rainfall amount, is also impacted by the size of supercooled droplets in the liquid layer lower in the cloud, which in turn depends on the abundance of available cloud condensation nuclei. In more polluted clouds, where more aerosol particles are available to nucleate cloud droplets, individual droplets will be smaller and will be collected less efficiently by falling ice crystals, thus reducing riming and total precipitation. Therefore, while increases in the number concentrations of aerosol particles that can act as cloud condensation nuclei are expected to decrease precipitation, by slowing coalescence of liquid droplets and riming onto ice crystals, enhanced INP numbers higher in the cloud could actually lead to increases in precipitation totals (Rosenfeld et al., 2014). Thus, to accurately represent the effects of aerosol particles on precipitation in models both the type of particles present and their location in the clouds must be known. Further, in the case of INPs, the temperature at which the particles can initiate freezing must be known. Analysis of precipitation during AR events in 2009 and 2011 sampled as part of the California Water (CalWater) campaign found that dust and biological particles, two important INP types but with very different freezing characteristics (Murray et al., 2012), were present and contributed to enhanced precipitation (Ault et al., 2011; Creamean et al., 2013).

The 2015 Atmospheric Radiation Measurement Cloud Aerosol Precipitation Experiment (ACAPEX) was designed to study the cloud and aerosol properties in landfalling ARs in California and the intense precipitation associated with these events. This study was part of the CalWater 2015 measurement campaign participated in by the U.S. Department of Energy, National Oceanic and Atmospheric Administration, National Science Foundation, and National Aeronautics and Space Administration (Ralph, et al., 2016). The campaign included sampling platforms on four aircraft, a ship, and at a coastal surface station. This project followed on the work done during CalWater campaigns in 2009, 2011, and 2014 (Ralph, et al., 2016).

As part of this study, our goal was to characterize INP concentrations, sources, and types associated with winter storms in California. As noted above, previous work has suggested that dust, associated with long-range transport from Asia, could be an important source of INPs during AR events. However, these long-range dust transport events are very episodic and might not always co-occur with AR events. Thus, other INP sources could also be important contributors to the INP budget during these storms. Specifically, oceanic aerosol could be a potential source of INPs (McCluskey et al., 2018; McCluskey et al., 2018), especially since these storm systems travel for thousands of miles over the ocean and are associated with strong onshore flow leading to increased wave breaking. However, these marine INPs, while biogenic (McCluskey, Ovadnevaite, et al., 2018), are much less efficient ice nucleators than dust or terrestrially-sourced biological (intended to

mean microbial herein) particles (DeMott et al., 2016), and thus could lead to different cloud and precipitation properties if they were the dominant or only INP source. Another potential INP source is local soil particles (Hill et al., 2016) lofted by increased winds associated with the landfalling storm. While some combustion sources, such as biomass burning, could also contribute to the INP population (Levin et al., 2016; McCluskey et al., 2014; Petters et al., 2009), Schill et al. (2016) found no emission of INPs from diesel combustion. Other anthropogenic emissions, such as sulfate and nitrate aerosol, while likely accounting for the majority of aerosol number in this region are not expected to contribute to the heterogeneous INP budget. To untangle these complex aerosol types and sources, during the 2015 study, we successfully measured INP concentration and aerosol composition directly as an AR approached and made landfall in northern California and moved up into the Sierra Nevada Mountains. In efforts to quantify the range of possible aerosol populations and their respective ice nucleation abilities, in this study we extended INP measurements to warmer temperatures and to lower detection limits than in previous studies. Over the course of the two-month study period we also measured INP concentrations and aerosol characteristics in the marine boundary layer, throughout the Central Valley, and up into the mountains under a variety of meteorological conditions.

2. Measurements

2.1. ACAPEX and CalWater 2015 Measurement Overview

We will focus our description on instruments used during the CalWater 2015 campaign (https://www.arm.gov/research/campaigns/amf2015apex). A similar suite of aircraft measurements were made during the CalWater 2011 campaign (https://www.arm.gov/research/campaigns/aaf2011calwater), although filter samples for off-line INP analysis were not collected in 2011. As part of ACAPEX, airborne measurements of aerosol and cloud properties were made aboard the Department of Energy Atmospheric Radiation Measurement Aerial Facility Gulfstream-I (G-1) aircraft (Schmid et al., 2014). The aircraft was based out of McClellan Airfield in Sacramento, CA. The G-1 performed 28 research flights between 16 January and 7 March 2015, as discussed below. Individual flights, or portions of flights, were focused on sampling over the open ocean, along the California shore, especially in the vicinity of the Bodega Bay surface site, throughout the Central Valley and over the Sierra Nevada Mountains east of Sacramento (Figure 1). There were also a large number of measurements in the vicinity of Sacramento as every flight began and ended at McClellan Airfield, located to the northeast of the city. Vertically, measurements were made from the surface up to ~7 km above sea level, with the majority of measurements made in the boundary layer, below 2 km. In addition to the aircraft measurements, a surface site was located at the UC Davis, Bodega Marine Laboratory in Bodega Bay, CA (Martin et al., 2017) and aerosol measurements were also made on the National Oceanic and Atmospheric Administration Ronald H. Brown research vessel which traveled from Hawaii to California during the study period.

2.2. INP Measurements

Real-time measurements of ice nucleating particle number concentrations (n_{INP}) were made with the Colorado State University (CSU) Continuous Flow Diffusion Chamber (CFDC) aboard the G-1. The CFDC-1H, which has been described in detail elsewhere (DeMott et al., 2015; Eidhammer et al., 2010; Rogers et al., 2001), uses a temperature and relative humidity controlled growth region to activate particles which are capable of nucleating ice at the set conditions and then grow them into ice crystals which can be easily detected using an optical particle counter (OPC, CLIMET 3100). The CFDC was operated with a 1.5 volumetric L/min sample flow confined within an 8.5 volumetric L/min sheath flow. Unfrozen droplets, representing the vast majority of sampled particles, are evaporated in the lower region of the CFDC where the relative humidity is adjusted to be below water saturation, while still at or above ice saturation, to allow for differentiation between ice crystals and non-INP aerosol based on size. The residence time in the growth region is approximately 5 s and the total residence time is approximately 7.5 s (DeMott et al., 2015). Both the sample and sheath flows were dried using two diffusion driers, the first containing silica gel and the second molecular sieves to prevent frost buildup inside the instrument. Large aerosols, which cannot be differentiated from ice crystals based on size alone, were removed upstream of the CFDC growth tube with dual 2.5-μm cut-size inertial impactors. For this project, all measurements were made above water saturation, typically at relative humidity = 105–108%, or 5–8%

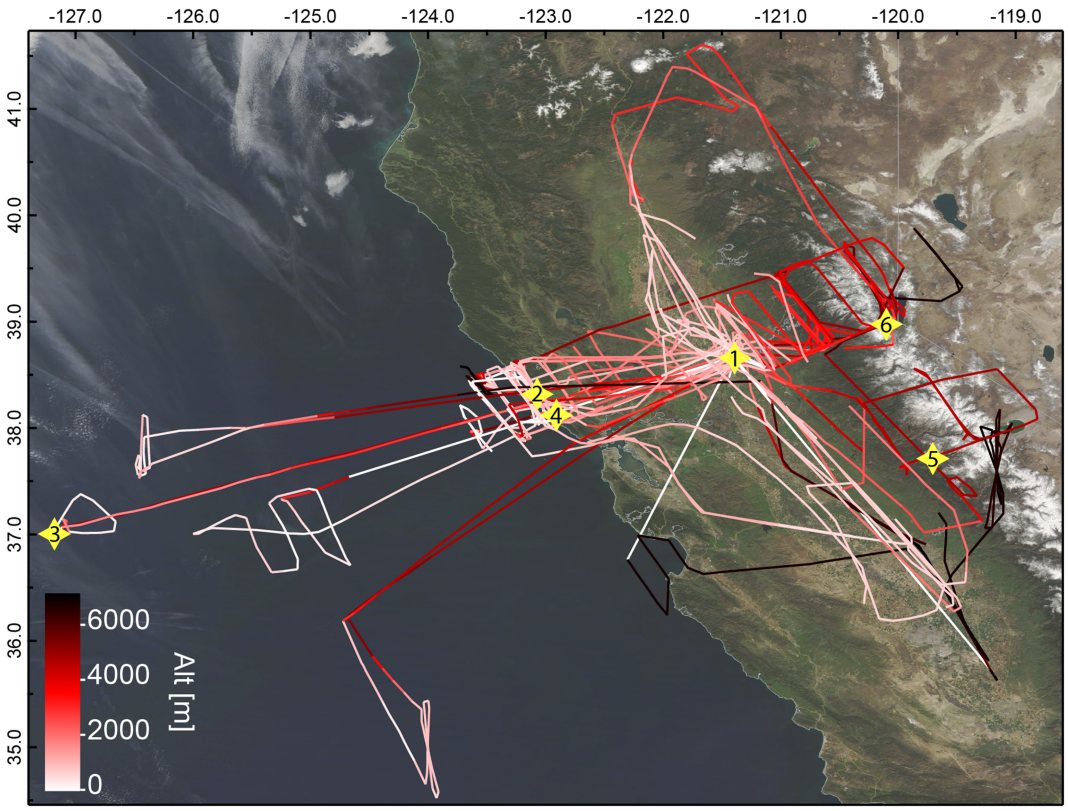

Figure 1. All flight tracks during ACAPEX colored by altitude. Yellow symbols show the locations of McClellan airfield (1), the Bodega Bay surface site (2), the location of the Ronald H. Brown during the AR event (3), and the IMPROVE sampling sites at Point Reyes (4), Yosemite (5), and Bliss State Park (6).

supersaturation with respect to water (s_w). At these conditions, aerosol particles take up water to form supercooled liquid droplets before freezing, if the particle is capable of ice nucleation at the set temperature. We were thus investigating condensation or immersion freezing, which are considered to be the dominant mechanisms of ice crystal formation in mixed-phase clouds (Hoose & Moehler, 2012). For this study, processing temperatures in the CFDC were varied between about −20 and −30 °C for different time intervals and all n_{INP} measurements are reported as a function of processing temperature. Sampled volumes were converted to standard L using the temperature and pressure inside the CFDC column and standard temperature and pressure of 0 °C and 1 atm.

Measurements of CFDC background counts were routinely made by sampling through a High-Efficiency Particulate Air (HEPA) filter. Background counts arise from frost flaking off the inner walls or inlet manifold of the CFDC. All CFDC sample data were background corrected by subtracting the interpolated filter measurement before and after each sampling period. Background corrected data were then averaged to 2-min sampling times to increase statistical confidence. If the sample line was switched between the two inlets (discussed below) during a 2-min sample period, the time periods when sampling from each inlet were averaged and reported separately. Sample data were considered to be statistically significant at the 95% confidence level if they were greater than 1.64 times the INP error, calculated by adding the Poisson counting statistics derived standard deviations from both the sample period and filter measurements in quadrature.

The CFDC sampled from two inlets on the G-1. An isokinetic inlet (hereafter ISO; Brechtel Manufacturing) was used to sample aerosol particles smaller than 5 μm in diameter when flying in clear air. When flying in clouds, droplets and ice crystals were collected by sampling through a counter-flow virtual impactor inlet (CVI; Brechtel Manufacturing) which allowed passage of cloud particles (i.e., droplets and ice crystals) with sufficient inertia to break through the counter flow barrier, or stagnation plane. For ACAPEX, the counter flow was set such that the cut size (50% penetration) averaged over all flights was 8.8 ± 0.46 μm in

diameter. Cloud particles sampled into the CVI were melted and evaporated with dry, heated air in the inlet allowing measurement of the residual aerosol particles which were present in the droplet or ice crystal. Note that ice and cloud droplet residuals are not necessarily the particles responsible for nucleation but could instead be particles that were scavenged by the ice crystal or droplet (Stith et al., 2011). When sampling though a CVI, particle concentrations are enhanced above ambient conditions due to the nonisokinetic flow. Enhancement factors were averaged over each CFDC sampling period and the CFDC data were corrected by dividing measured INP concentrations by the enhancement factor. While it did vary with altitude, over all cloud measurement periods during ACAPEX the average (±1 standard deviation) CVI enhancement factor was 13.1 ± 3.5.

Filters were also collected aboard the aircraft as well as on the Ronald H. Brown and at Bodega Bay for subsequent INP analysis with the CSU Ice Spectrometer (IS), which can investigate immersion freezing across a temperature range of 0 to about −27 °C (Hill et al., 2016; Hiranuma et al., 2015). On the G-1, filter samples were only collected from the ISO inlet and individual filters were collected during level flight legs or over multiple legs at similar altitudes and in the same air mass. Forty-nine filter samples were collected from the G-1 over the course of the study with a median sample volume of 119 L. Aerosols were collected at a median of 2.7 L/min through a 47-mm-diameter in-line aluminum filter holder (Pall) fitted with a 0.05-μm-pore-diameter Nuclepore polycarbonate membrane (Whatman) overlying a 3-μm-pore-diameter Nuclepore polycarbonate backing membrane (to avoid any potential contamination of INPs from the support grid). Disassembled filter holders were cleaned by soaking in 10% H_2O_2 for 60 min followed by rinses in deionized water (18 MΩ and 0.2-μm pore diameter filtered) and removal of excess water with a compressed gas duster before air-drying in a clean, plastic tub. On the Ronald H. Brown and at Bodega Bay, precleaned filters were preloaded into sterile, open-faced Nalgene filter units (Thermo Fisher Scientific Inc.) and placed beneath a rain shield secured on the ship's outboard railings and on top of the sampling trailer. Prior to the study, all sample collection filters were cleaned in a laminar flow cabinet (<0.01 particles cm^{-3} larger than 10 nm in diameter) by soaking in 10% H_2O_2 for 10 min followed by three rinses in deionized water, the last of which had been filtered through a 0.02-μm-pore-diameter filter (Anotop 25-mm syringe filter, Whatman) and drying on foil (McCluskey et al., 2017).

After sampling, filters were transferred to and from filter holders and Nalgene units using cleaned (same as for filters) plastic forceps (Fine Science Tools) and stored at −20 °C in 60-mm-diameter petri dishes (CELLTREAT). For re-suspension of particles, filters were placed in sterile 50-mL Falcon polypropylene tubes (Corning Life Sciences), 5–6 mL of 0.02-μm-pore-diameter filtered deionized water added (which contained, on average, 3.7 INPs mL^{-1} at −25 °C) and particles re-suspended by tumbling on a Roto-Torque (Cole-Palmer) at 60 cycles/min for 20 min. Within a laminar flow cabinet, 32 × 50-μL aliquots of each suspension were transferred into sterile, 96-well PCR trays (Life Science Products Inc.), and the plates were transferred to the IS blocks (McCluskey et al., 2017).

Immersion freezing temperature spectra were obtained from the IS following previously documented procedures (Hiranuma et al., 2015). Frozen wells were monitored as temperature was lowered at 0.33 °C min^{-1} under aspiration of the instrument headspace with 0.5–1 L/min of cooled, filtered (HEPA-CAP, Whatman) nitrogen. Frozen wells were counted at 0.5 or 1 °C degree intervals to a limit of −27 °C, and cumulative numbers of INPs mL^{-1} of suspension were estimated using

$$INPs\ mL^{-1} = \frac{-\ln(f)}{V} \tag{1}$$

where f is the proportion of droplets not frozen and V is the volume of each aliquot (Vali, 1971). Given the number of wells and liquid volumes used here for the aircraft samples, the lower detection limit, defined as the occurrence of one freezing event, was about 3.2 INP/filter. Filter blanks (loaded into in-line filter units and loaded into and removed from the sampling platform) were processed to obtain background INP spectra. All gave broadly similar results, and the highest was chosen as the field negative to provide conservative estimates of atmospheric INP concentrations. At each temperature, INPs in the blank were subtracted from sample measures in suspension, and then measured INPs in the total volume of suspension were converted to INPs L^{-1} using the liters of air sampled. Binomial sampling confidence intervals (95%) were derived using the formula recommended by Agresti and Coull (1998):

$$CI_{95\%} = \left(\widehat{p} + \frac{1.96^2}{2n} \pm 1.96\sqrt{\left[\widehat{p}(1-\widehat{p}) + {}^{1.96^2}/_{4n}\right]/n}\right) / \left(1 + {}^{1.96^2}/_{n}\right) \quad (2)$$

where $\widehat{p}$ is the proportion of droplets frozen and n is the total number of droplets.

2.3. Aerosol Chemical Composition

The vacuum aerodynamic diameter (calibrated for d_{va} = 0.27–1.3 μm) and chemical composition of individual particles was measured using an aircraft aerosol time-of-flight mass spectrometer (A-ATOFMS, hereafter ATOFMS) onboard the G-1. The same valve controlled the inlet selection, either ISO or CVI, for both the CFDC and ATOFMS on the G-1, so that both instruments were always measuring the same sample. Detailed descriptions of the ATOFMS have been previously published (Pratt et al., 2009) and only a brief description is provided here. At the inlet of the instrument, particles are first drawn through a ^{210}Po neutralizer (1U400, Amstat Industries, Inc., Glenview, IL; 1.5 mCi 0.08 cm^3) and pressure-controlled inlet into an aerodynamic lens. This collimated particle beam is focused through two orthogonal, continuous wave 532-nm lasers spaced 6 cm apart. When particles travel through each of these laser beams, they scatter light, which is collected by an ellipsoidal mirror and focused onto a photomultiplier tube. The time lag between detection of the two scattering events is used to determine vacuum aerodynamic diameter based on calibration with polystyrene latex spheres of known diameter. Particles are then desorbed and ionized using a Q-switched, frequency quadrupled Nd:YAG laser operated at 266 nm with an 8-ns pulse width and 700-μm spot diameter. The resulting ions then enter a dual-polarity time-of-flight mass spectrometer generating both a positive and negative mass spectrum.

Raw spectral data from the ATOFMS were imported into Matlab (MathWorks, Inc.) and analyzed using the single-particle mass spectrometer analysis toolkit FATES (Sultana et al., 2017). Chemically similar mass spectra were grouped using an adaptive neural network (ART-2a, vigilance factor of 0.8, learning rate of 0.05, 20 iterations, and a regroup vigilance factor of 0.85 (Rebotier & Prather, 2007; Song et al., 1999)). Spectral clusters were assigned to particle types based upon similarity to previously defined types from prior field and laboratory studies. For this analysis, we then grouped these clusters into nine aerosol source classifications based on the dominant components of each cluster. These aerosol source classifications were sulfate/nitrate, biomass burning, marine aerosol, elemental carbon (EC), organic carbon (OC), dust, biological particles, metals, and other aerosol components. Table 1 shows the top 19 particle types measured by the ATOFMS and their corresponding aerosol source classifications. Note that particles containing stainless steel, which could indicate inlet contamination and accounted for <0.1% of measured particles, were excluded from this analysis. Relevant to later discussion, there is a chance that marine microbial INPs could be present within the biological category, but on a surface area basis, marine INPs are at most times likely to be primary marine biogenic particles most related to the other marine aerosol categories that are dominated by sea salt (McCluskey, Ovadnevaite, et al., 2018).

2.4. Other Measurements

In addition to aerosol composition measurements from the ATOFMS, we also use measurements of bulk $PM_{2.5}$ aerosol composition from IMPROVE network monitoring sites at Point Reyes station, on the coast ~16 km south of Bodega Bay (lat = 38.1224, lon = −122.9085, alt = 97 m above sea level) as well as Bliss State Park, on the western side of Lake Tahoe (lat = 38.9761, lon = −120.1024, alt = 2,130.67 m above sea level) and Yosemite National Park (lat = 37.7133, lon = −119.7061, alt = 1,603 m above sea level). The IMPROVE sampler, described by DeBell et al. (2006), consists of four modules, each with its own pump, size cutting cyclone, and sample substrate. Three modules have a 2.5 μm aerodynamic size cut ($PM_{2.5}$) and collect aerosols onto Teflon, nylon, and quartz filter substrates, respectively. The fourth module uses a 10 μm aerodynamic size cut (PM_{10}) and collects particles onto a Teflon filter. The two Teflon filters are weighed before and after sampling in a clean, climate-controlled room kept at a relative humidity of 20–40%, to determine total gravimetric mass loading. The $PM_{2.5}$ Teflon filter is also analyzed by X-ray fluorescence analysis for the common soil elements Al, Si, Ca, K, Fe, Ti, Mg, and Na. Concentrations of NO_3^- and SO_4^{2-} are determined by IC analysis of an aqueous extract of the nylon filter, and the quartz filter is analyzed via thermal optical reflectance for organic and elemental carbon. Following the IMPROVE algorithm, the measured elemental crustal components were used to calculate the mass of soil, or dust, aerosol as follows:

Table 1
Particle Types Measured by the ATOFMS and Source Classifications

Cluster	Particle type	Identifying peaks/notes	Classification
1	Marine organic oligomers	Organic high mass oligomer peaks 250–500 m/z in negative and positive with separations of 14 m/z Also contains sulfate, salt, organic nitrogen (CN^- and CNO^-), phosphate (PO_2^- and PO_3^-)	Marine
2	Salt (fresh)	Salt peaks (Na_xCl_y)—a little NO_3^- present on some particles	Marine
3	Salt (aged)	Minor salt peaks, sodium nitrate peaks, nitrate peaks	Marine
4	Biomass burning (K)	Potassium (K^+) dominant, K_2HSO_4, K_3SO_4	Biomass burning
5	Biomass burning (carbonaceous)	Potassium, C_3^+, $C_2H_3O^+$, C_4^+, $C_4H_3^+$, C_5^+, $C_5H_3^+$	Biomass burning
6	Elemental carbon (EC)	C_n^+ and C_n^- peaks	EC
7	EC/OC aged soot	Dominant C_3^+peak, minor C^+, K^+, $C_2H_3O^+$, C_4^+, C_5^+	EC
8	Organic carbon (OC)	$C_2H_3^+$, C_3^+, C_3H^+, $C_2H_3O^+$, $C_4H_2^+$, $C_4H_3^+$, $C_5H_3^+$, $C_6H_5^+$,	OC
9	Highly processed nitrate	Neg spectra only, nitrates NO_3^-, H $(NO_3)_2^-$, NO_2^-	Sulfate/nitrate
10	Highly processed sulfate/nitrate	Neg spectra only, nitrates NO_3^-, H $(NO_3)_2^-$, NO_2^- and sulfate HSO_4^-	Sulfate/nitrate
11	Sulfate/sulfuric acid	HSO_4^- and/or $H_2SO_4HSO_4^-$	Sulfate/nitrate
12	HMOC (high-mass organic carbon)	High mass peaks in positive spectra, intense K peak, nitrate and sulfate peaks Not to be confused with marine organic oligomers	OC
13	Silicates (dust)	Particles containing silicate peaks SiO_3^-, SiO_2^-, Si_2O^- various positive ion peaks (Fe^+, Al^+, Ca^+, Ba^+, Co^+, K^+, Ti^+)	Dust
14	Metal containing particles	Spectra containing intense metal peaks (Ca^+, Cr^+, Ba^+, Al^+, Mo^+, Sn^+, Co^+, As^+, Ag^+, Zr^+, Cu^+) without other conclusive identifying peaks	Metals
15	Lead particles	Lead dominating peaks ($206/207/208^+$)	Metals
16	Calcium dust	Ca^+, $CaO/CaOH^+$, Ca_2O/Ca_2OH^+, $(CaO)_2/(CaO)_2H^+$	Dust
17	Vanadium particles	V^+ and VO^+	Metals
18	Biological	Particles containing significant PO_3^-, PO_2^-, CNO^-, and CN^- Variety other peaks also present	Bio
19	K^+	K rich or K^+ only	Biomass burning
23	Stainless steel	Cr^+, Fe^+, Ni^+, and Mo^+ (inlet artifact)	N/A
30	Unidentified		Other

$$[\mathrm{SOIL}] = 2.2[\mathrm{Al}] + 2.49[\mathrm{Si}] + 1.63[\mathrm{Ca}] + 2.42[\mathrm{Fe}] + 1.94[\mathrm{Ti}] \quad (3)$$

where the terms are mass concentrations of aluminum, silicon, calcium, iron, and titanium, and the coefficients account for the common oxides of these soil elements (Malm et al., 2004). Following the standard IMPROVE network sampling schedule, samplers were collected for 24 hr every third day.

A number of instruments on the G-1 measured aerosol, cloud, and precipitation properties. Here we will just mention those instruments used for this analysis. Aerosol total number concentrations (n_{tot}) were measured with Condensation Particle Counters (TSI 3010) continuously on both the ISO and the CVI inlets. We used the total number concentration measured by the CPC from the corresponding inlet, averaged over each CFDC sample period, to calculate temperature dependent ice nucleating efficiency (ξ_T) following Petters et al. (2009):

$$\xi_T = \log_{10} \frac{n_{INP}}{n_{tot}} \quad (4)$$

In situ aerosol size distributions were measured with wing-mounted optical detectors. An Ultra High Sensitivity Aerosol Spectrometer (UHSAS; Droplet Measurement Technologies) measured aerosol particles from 0.067 to 1.1 μm in diameter and a Passive Cavity Aerosol Spectrometer (PCASP; Droplet Measurement Technologies) measured between 0.1 and 3.0 μm. We combined data from these two instruments to create continuous size distributions between 0.07 and 2.5 μm, using PCASP data at sizes larger than the UHSAS detection limit. We used 2.5 μm as the upper limit for the combined size distribution, although the PCASP can measure larger sizes, to match the upper (50%) size-cut of the CFDC measurements. To

account for hygroscopic growth of aerosol particles, we calculated dry aerosol size distributions from the combined UHSAS-PCASP measurements using Köhler theory and an assumed hygroscopicity parameter (κ; Petters & Kreidenweis, 2007) of 0.2 for terrestrial dominated aerosol and 0.7 for marine dominated aerosol (as determined by the presence or absence of marine aerosol in the ATOFMS data; Petters & Kreidenweis, 2007). We then used these dry number size distributions to calculate total aerosol surface area (s_{tot}) averaged over each CFDC sampling period. Uncertainties in sizing from the optical probes results in a surface area uncertainty of about 30% (Kupc et al., 2018). These s_{tot} values were subsequently used to calculate the INP surface site density (n_s; DeMott et al., 2016; Niemand et al., 2012) as follows:

$$n_s = n_{INP}(T)\frac{10^9}{S_{tot}} \tag{5}$$

where n_s has units of m^2, n_{INP} of L, and s_{tot} of $\mu m^2/cm^3$. Because the PCASP and UHSAS are wing mounted probes, which cannot be trusted in clouds due to severe cloud element shattering in inlets, we can only use the data to determine aerosol size distributions, and surfaces area, in clear air, and thus only report n_s for clear air samples. We also note that the site density approach is only strictly valid when INPs are of a single assumed type. We compute values here, recognizing that they may reflect multiple INP compositions at any time, but that the values with respect to a certain composition would strictly have to be parsed out for comparison to previous assessments, requiring procedures (Cornwell, 2019) not applied on the G-1. This is discussed further in section 3.

Atmospheric variables, such as temperature, pressure, and relative humidity as well as aircraft state (altitude, position, airspeed, etc.), were all constantly measured on the G-1, as described by Schmid et al. (2014), and are used in this analysis.

3. Results and Discussion

3.1. Overview of INP Measurements

Across the entire ACAPEX study, number concentrations of INPs (n_{INP}) ranged from near 0 up to a few ~10s L^{-1} at temperatures from −20 to −30 °C (Figure 2), which are typical for ambient n_{INP} values at these temperatures in relatively clean environments (DeMott et al., 2010). While concentrations as high as 100–1,000 L have been observed in heavily dust impacted environments (Boose et al., 2016; DeMott et al., 2015) and 100s L^{-1} in agricultural areas during harvesting (Suski et al., 2018), no such high values were observed during this study. There was considerable variability in n_{INP} during each flight, with the range in n_{INP} values during any given flight greater than the range in average n_{INP} across all flights, even in cases where CFDC measurements were only made over a narrow temperature range, illustrated in Figure 2. As well as variability in n_{INP}, the fraction of total aerosol particles capable of ice nucleation at a given temperature (ξ_T) and INP surface site density (n_s) were also highly variable during every flight (Figure 2). Averaged across each flight, values of ξ_T at −30 °C ranged from about −6 to −4 with a mean (±1 standard deviation) of −5.6 ± 1.2. Previous measurements of known INPs, using kaolinite and Arizona Test Dust, had ξ_T values between −2 and −4 at −30 °C while biomass burning emissions, which are relatively poor ice nucleators compared to dust, had values around −6 to −10 at similar temperatures (Levin et al., 2016). The variability and range of n_s values is discussed in greater detail below in the context of INP type.

We also evaluated the vertical distribution of INPs, INP efficiency, and site density, shown in Figure 3, for both clear air and cloud measurements. Over the entire study, altitude averaged processing temperatures were similar with a standard deviation of 0.95 °C. The maximum difference in average temperatures was −26.88 °C (±3.1 °C) at 5,500 m to −29.63 °C (±2.9 °C) at 6,500 m. While there was a large spread in n_{INP} and ξ_T across altitude levels, we did observe an increase in n_{INP} (converted to standard L) with altitude, with median values increasing from 1.5 to 5.3 L^{-1} from 500 to 6,500 m. Median ξ_T values also increased with altitude, from −6.3 to −4.9 for measurements made in clear air, possibly due to the fact that pollution aerosol, which are at higher concentration near surface sources, are poor INP (Chen et al., 2018). These changes were both statistically significant at the 95% confidence level, as determined using a two-tailed t test. For measurements made in cloud, from the CVI, there was even more scatter in n_{INP} with no statistically significant changes with altitude. There was, however, a significant increase in ξ_T with altitude, similar to that seen for the interstitial aerosol.

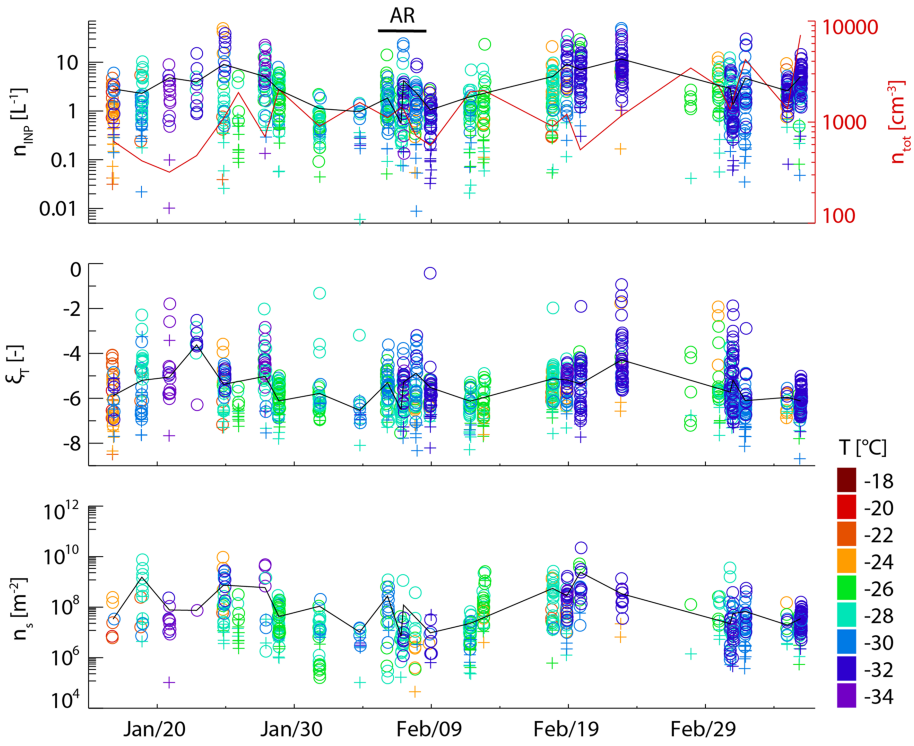

Figure 2. (top panel) Timeline of all n_{INP} measurements made with the CFDC colored by sample processing temperature for all ACAPEX flights. Circles represent data when n_{INP} values were above the 95% confidence threshold for statistical significance, while crosses show data below this threshold. (top) Total aerosol concentrations (n_{tot}) measured by a CPC sampling from the isokinetic inlet, as well as (middle) ξ_T and (bottom) n_s colored by processing temperature are also shown. Solid black lines (continuous only to guide the eye) show flight averaged values at −30 °C (±2.5 °C).

For any given aerosol population, ice nucleating ability is strongly dependent on temperature with the number of available INPs for particle types such as mineral dust or sea spray aerosol typically increasing exponentially as temperature decreases. Figure 4 shows n_{INP} (standard L^{-1}) measured by both the CFDC and IS filters in clear air for the entire ACAPEX study from aircraft measurements. As expected, there was an increase in n_{INP} with decreasing temperature. However, again, there was considerable scatter in the data, especially for the CFDC measurements, indicating that changes in measured n_{INP} were driven by variability in overall concentration, and not just processing temperature during this study. As with previous studies (DeMott et al., 2017), we also observed good agreement, in general, between n_{INP} measured by the CFDC and the IS, with the respective cloud of values falling on top of each other in the region of overlapping temperatures. Figure 4 also shows the CFDC data measured from the G-1 during the CalWater 2011 campaign, hereafter CalWater-1 (blue circles). Below −20 °C, the CalWater-1 data points all fell within the range measured during ACAPEX and there were no statistically significant differences in the mean n_{INP} values at −25 or −30 °C. At warmer temperatures, however, the CalWater-1 n_{INP} measured by the CFDC were relatively higher than those measured during ACAPEX with the IS, although with large uncertainties. We did not collect filters for IS analysis during CalWater-1, which allow for more reliable measurement of low n_{INP} at warm temperatures (i.e., lower detection limit).

Figure 5 is similar to Figure 4 but shows composite n_s as a function of temperature for all airborne measurements made during ACAPEX and CalWater-1. Comparing INP surface site density (n_s) as a function of temperature is a good way to investigate INP types as these n_s spectra have been determined for many different specific INP types (Murray et al., 2012) and normalize for aerosol abundance. To add some context to the n_s values measured during ACAPEX, two lines representing fits to mineral dust data (Ullrich et al., 2017) in orange and clean marine data (McCluskey, et al., 2018) in purple are also shown. While the "dust fit" line was calculated based on laboratory measurements of pure dust samples, DeMott et al. (2015) showed that atmospheric dust samples agreed well with laboratory parameterization of INP activation properties.

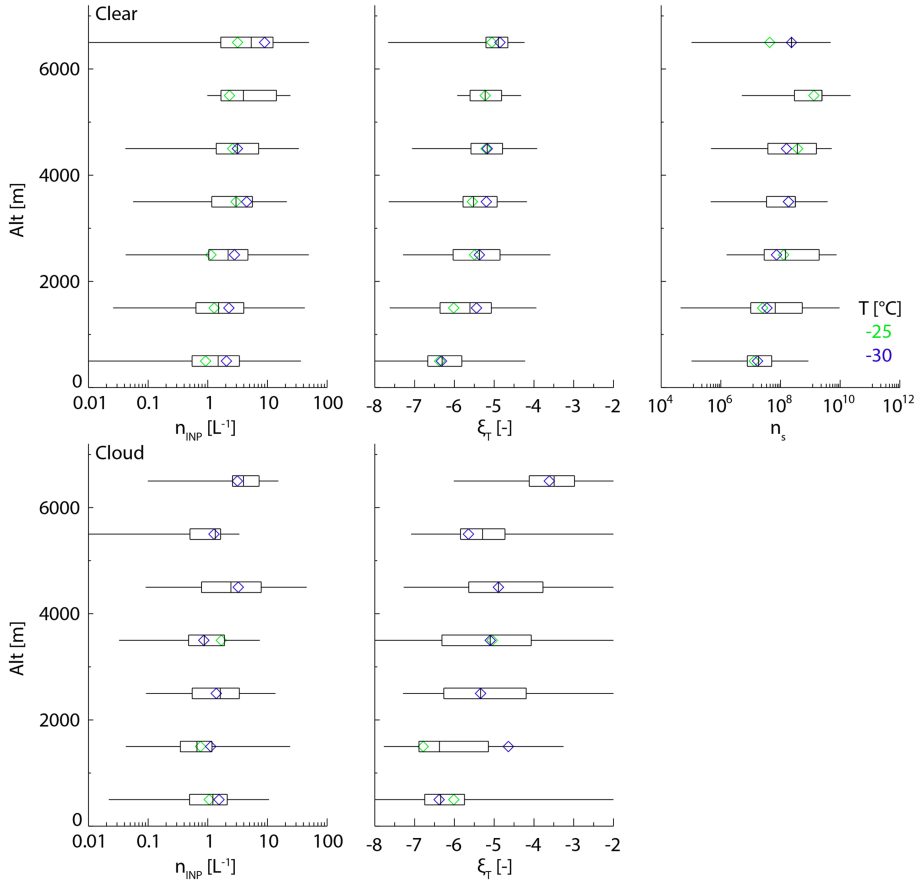

Figure 3. (left) n_{INP}, (middle) ξ_T, and (right) n_s for the entire ACAPEX campaign as a function of altitude measured from the (top) isokinetic inlet in clear air as well as (left) n_{INP} and (middle) ξ_T measured from the (bottom) CVI in clouds. Boxes show the 25th–75th percentiles for each 1,000-m vertical layer, with whiskers extending to the minimum and maximum values. Median values for all measured data (above the lower detection limit) are shown by thick black lines and median values for measurements made by the CFDC at −25 °C and −30 °C (±2.5 °C) are shown by the colored diamonds. Note that INP number concentrations are reported in standard L to allow for direct comparison across altitudes.

Ullrich et al. (2017) represents a correction to Niemand et al. (2012) in describing the results of mineral dust n_s in laboratory studies. DeMott et al. (2015) showed that the CFDC undercounted dust INP by a factor of 3, at the conditions under which we were operating during this study, when compared with the Niemand et al. (2012) parameterization. Thus, we also show the Niemand et al. (2012) dust fit line reduced by this factor (dashed line) to match what the CFDC would be expected to measure for dust INPs. We also note that the "clean marine fit" is thought to represent exudate marine INPs, versus microbial, heat-labile, episodic INPs that are active at warmer temperatures (McCluskey, et al., 2018). The vertical purple bars show the range in values from DeMott et al. (2016), a separate clean marine INP data set that was not used to generate the McCluskey et al. paramaterization.

For ACAPEX, 73% of the n_s points fell between the dust and clean marine fits, although with more data points near the clean marine line and few points close to or above the dust line. There was also considerable scatter in both the ACAPEX and CalWater-1 n_s values. Because ambient INP populations can be composed of many different aerosol types, each with different relationships between surface area and ice nucleating ability, we do not necessarily expect to see a clear trend with temperature, as we would for individual, homogeneous aerosol types. Especially with ambient data collected over many weeks with varying locations and under changing meteorological and aerosol conditions, as was the case during ACAPEX, there can be large changes in aerosol types and thus n_s values. However, these relationships between n_s and T can still provide useful information about dominant INP types. For example, values that fall on or near the clean marine line

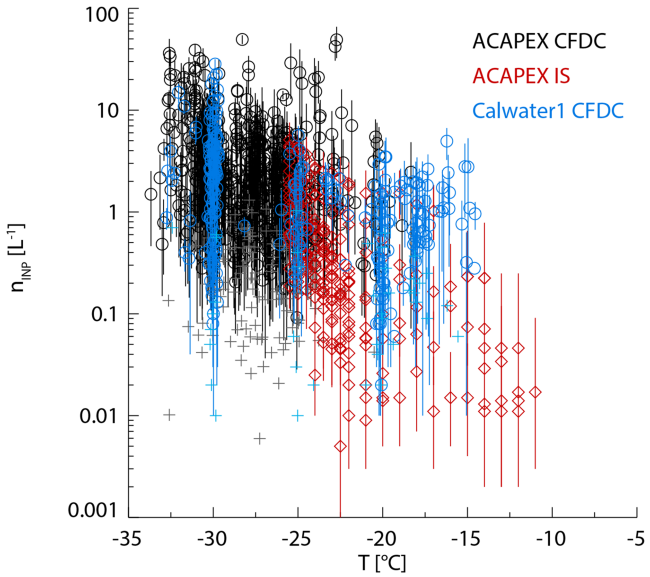

Figure 4. All airborne n_{INP} measurements (standard L^{-1}) from the CFDC (black) and IS (red) during ACAPEX and CFDC measurements from CalWater-1 (blue) as a function of temperature. For the CFDC data, circles represent points above the 95% confidence limit and lighter colored crosses show measured points below this threshold. Uncertainty bars show the 95% confidence intervals (see text).

likely would not include any dust INP. However, if any dust or other more active INP type were present, we would expect an n_s value above the clean marine line, even if it was still below the pure dust line. Thus, while the ACAPEX and CalWater-1 n_s values that fall between the two parameterization lines are due to a mixture of INP types, they likely indicate the presence of some dust or other nonmarine INPs impacting clouds at times during the study (Cornwell, 2019).

3.2. Overview of Aerosol Composition

While changes in n_s as a function of temperature can indicate differences in INP types, we also have direct measurements of aerosol chemical composition in the roughly 0.1- to 1-μm size range from the ATOFMS onboard the G-1. However, it must be noted that INPs make up a very small fraction of the total aerosol number (~1 in 10^5; Figures 2 and 3); thus, measurements of total aerosol composition are likely to be dominated by non-INPs, with the particles responsible for ice nucleation accounting for a tiny fraction of the total signal. However, these measurements are valuable in determining relative contributions of various aerosol types to the total population and, along with other measurements such as n_s, can help to constrain INP composition and source.

Over the entire campaign, marine aerosol and sulfate/nitrate aerosol (likely from anthropogenic pollution) each accounted for roughly one third of the total measured aerosol number, with biomass burning aerosol and EC particles comprising most of the remainder (Figure 6). However, when split between clear air and cloud there was a distinct difference in aerosol composition. This difference was partly driven by the different flights in which clear air or cloudy conditions were encountered. A large fraction of in-cloud measurements were made during the AR event when marine aerosol was by far the most dominant aerosol component measured by the ATOFMS. This will be discussed in more detail below. By contrast, many of the clear air flights were performed through the CA Central Valley, where anthropogenic emissions are expected to be a dominant aerosol source.

To investigate the variability in aerosol composition, the aerosol classification contributions were determined for each flight, shown in Figure 7. As noted above, during the AR event from 5 to 7 February, the aerosol composition was dominated by marine aerosol, with these components accounting for more than two thirds of the measured aerosol during this time period. During the first flight, on 16 January, marine aerosol was also the dominant component. This flight was also largely in cloud in AR conditions just off the coast or

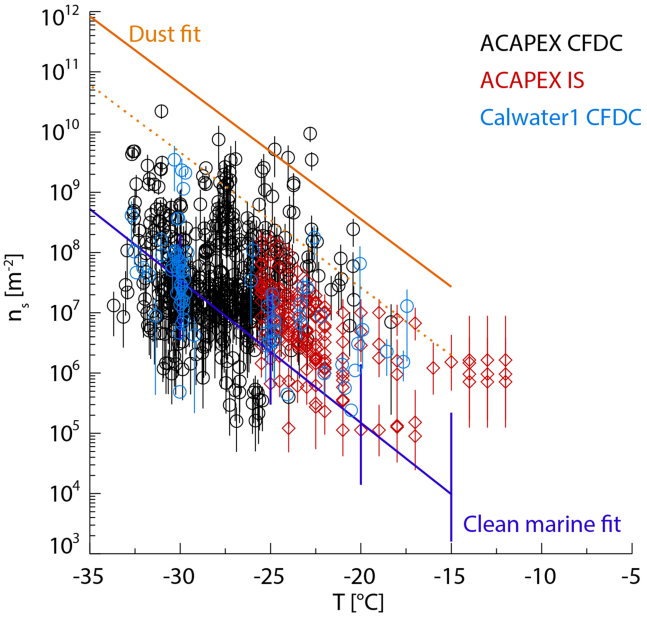

Figure 5. INP surface site density (n_s) as a function of temperature measured in clear air from the G-1 during ACAPEX from both the CFDC (black circles) and IS (red diamonds) and from the CFDC during CalWater-1 (blue circles). To add context the solid orange line shows a fit to laboratory data for dust INP (Ullrich et al., 2017) with the dashed orange line showing expected CFDC measurements of dust n_s values (DeMott et al., 2015; Niemand et al., 2012). The purple line shows a fit to clean marine data (McCluskey, et al., 2018) with the vertical purple lines showing the range of values found by DeMott et al. (2016) for marine INPs from both field and laboratory experiments. These reference values would be valid if all particles dominating surface area and the INP population were of a single compositional type and behaved as INPs as in these previous studies.

over the Bodega Bay surface measurement site. By contrast, the last two flights were flown through the southern Central Valley, between Sacramento and Bakersfield, almost entirely in clear air and the aerosol composition was dominated by pollution (sulfate and nitrate aerosol) and biomass burning emissions.

Notable in the ATOFMS measured aerosol composition is the relative lack of either biological aerosols or dust compared to other aerosol classes. These are both known ice nucleating particle types with certain terrestrial biological particles tending to dominate at temperatures between −5 and −20 °C and dust particles at temperatures below this (Hoose & Moehler, 2012; Murray et al., 2012) and were shown to be associated with enhanced precipitation during a large AR event sampled during CalWater-1 (Creamean et al., 2013; Creamean et al., 2014). While even a small number of these particles could greatly contribute to the INP population, during the ACAPEX AR event, the ATOFMS measured less than 1% dust or biological particles either from cloud residuals or in clear air above or below cloud base. In fact, throughout the entire study, dust particles were only a significant contributor to measured aerosol composition during one flight, on 1 March above the Sierra Nevada east of Sacramento. While most of the dust impacted period was in cloud, where we did not have surface area measurements and thus could not determine n_s, there were two CFDC measurement periods in the dust plume outside of cloud where n_s could be calculated. During these measurement periods, about one third of the aerosol number measured by the ATOFMS were calcium dust (cluster #16 in Table 1) with most of the remainder accounted for by pollution aerosol. These particles also accounted for about one third of the aerosol surface area measured by the ATOFMS. Using the total measured surface area, the average n_s during this time period was 2.8×10^7 m^2 at −25.3 °C, slightly above the top of the range of marine n_s (2.1×10^7 m^2 at −25 °C). We can calculate the upper bound of n_s for this dust type by assuming that it only comprised one third of the total surface area, that is, assuming that the fractions measured by the ATOFMS are consistent across the entire size distribution. Doing this results in an average n_s value of 8.4×10^7 m^2, which is still well below the adjusted dust parameterization at this temperature (1.0×10^9 m^2). Nevertheless, we note that Cornwell (2019) found a similar difference between explicitly calculated dust n_s and the Niemand et al. (2012) dust parameterization during dust periods that occurred in the marine boundary layer at the Bodega Bay coastal site during ACAPEX.

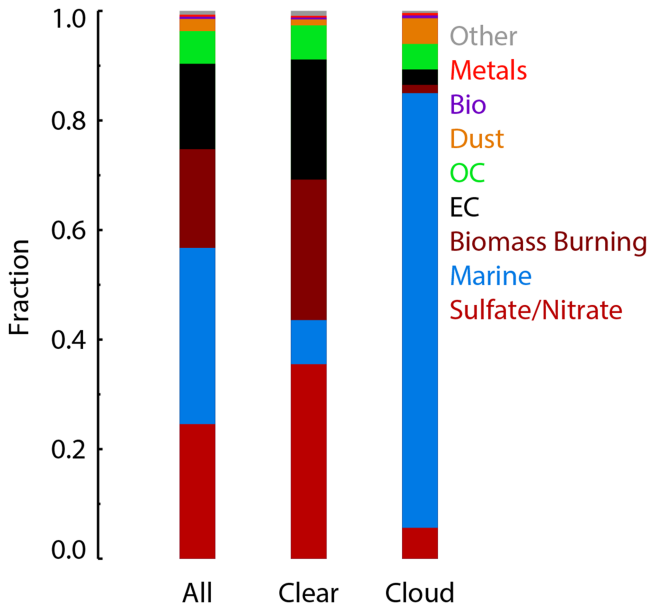

Figure 6. Fractional number contributions of nine aerosol classifications to the total, clear, and cloud sampling periods measured during the entire ACAPEX campaign. See Table 1 for aerosol source classifications.

3.3. Atmospheric River Event

On 6–7 February 2015, an AR made landfall on the coast of Northern California bringing heavy rainfall with some regions receiving 100–400 mm of total precipitation during the event (Cordeira et al., 2017; Ralph et al., 2017). We sampled in the AR during four flights as it was approaching the coast and making landfall. On 5 February, before the AR made landfall, the G-1 flew at an elevation of ~250 m over the Ronald H. Brown research vessel, which was located about 420 km offshore (lat = 37.004, lon = −127.179). We also sampled in clear air at an elevation of 5 km as we transited to the rendezvous point with the ship. Over the ship, at low elevation, the flight track was almost entirely in warm cloud with cloud temperatures of about 5–10 °C. On 6 February, as the AR made landfall, we flew two flights, one just off shore of the Bodega Bay surface site and one up into the Sierra Nevada Mountains east of Sacramento. The second flight pattern was repeated on 7 February.

During the AR event, n_{INP} measured on the G-1 were generally very low, especially when flying in cloud over the ocean on 5 February when the IS measured some of the lowest n_{INP} values of the campaign (Figure 8a). Although values were low, during the AR event there was an increase in n_{INP} when moving from the open ocean toward the shore. This was seen clearly in the IS measurements made aboard the Ronald H. Brown and at Bodega Bay as well as from the G-1 IS data (Figure 8a). Circles in Figure 8a show G-1 data with blue points measured when the aircraft was over the ship (squares) on 5 February, and green points when the aircraft was flying parallel to the coastline just off shore of Bodega Bay (diamonds), at 550 m above sea level, on 6 February. The aircraft points agreed very well with those measured on the ship and were slightly lower than those measured at the Bodega Bay surface site. This could be due to the fact that flights were required to be at higher altitude near the shoreline than when over the open ocean, and thus were further from surface-based aerosol sources. Further, surface-based filters were collected for 24 hr, while aircraft samples were only collected for 10–20 min, which could lead to some discrepancies. Ship-based IS measurements are also included for 6 February in Figure 8a and show no significant change in n_{INP} compared to 5 February. The major source of aerosols during this event was from the ocean (discussed below), which was likely enhanced by near-shore and surf-zone wave action and could be a reason for the increase in n_{INP} at the Bodega Bay surface site.

While n_{INP} were generally low during the AR event, after the storm passed we observed an increase in n_{INP}. Most notably, from IS data collected on the G-1 and at the Bodega Bay site on 11 February, we observed an increase in n_{INP} at temperatures warmer than −20 °C (red points in Figure 8a) to the highest values

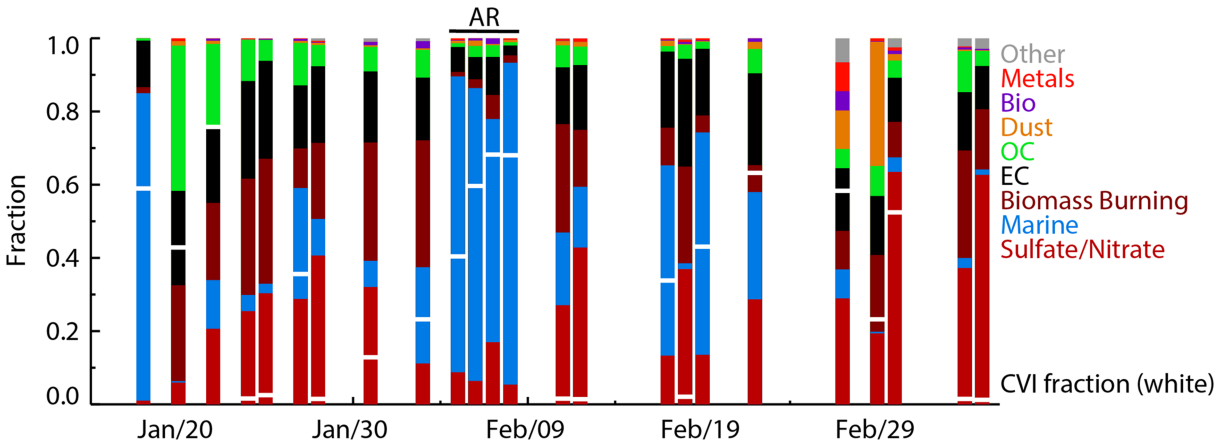

Figure 7. Fractional number contributions of aerosol source classifications (Table 1) based on composition data from the airborne ATOFMS for each flight in all sampling conditions (in cloud and clear). White bars indicate the fraction of sampling time on the CVI inlet (i.e., fraction of time in cloud) and are plotted on the same *y* axis as the number fractions.

measured during the study at these temperatures. The red filled and open circles in Figure 8a show data collected just offshore of the Bodega Bay site (alt = 100 m) and in the southern Central Valley (lat = 37.04, lon = 120.7, alt = 440 m), respectively, showing the large spatial extent of this enhanced INP event. Filter measurements from the Central Valley on 12 February (not shown) were also very similar to those on 11 February in this region. This increase in n_{INP} at these relatively warmer temperatures is commonly indicative of terrestrial biological INPs (Petters & Wright, 2015; Suski et al., 2018) and back trajectory analysis during this time period (Figure 8b) clearly showed air masses intercepting the terrestrial boundary layer prior to arrival at the Bodega Bay site (red lines). Previous studies have observed an increase in n_{INP} following rain events associated with an increase in such terrestrial biological particle concentrations (Huffman et al., 2013; Prenni et al., 2013; Tobo et al., 2013), suggesting that intense rains have a feedback effect on the production and release of INPs (Morris et al. 2019), as observed here. This is demonstrated specifically for the Bodega Bay site by Cornwell (2019). In that study, the variability in n_{INP} trended with the abundance of particles containing bioaerosol markers measured by a Wideband Integrated Bioaerosol Sensor (Wright et al., 2014) and a separate ATOFMS deployed at the ground site. That these same enhancements in INPs were seen throughout the boundary layer for several days following this AR event during ACAPEX suggests that there was widespread production of biological INPs on vegetation (Hirano et al., 1996) and/or in soil in response to the rain event.

In agreement with back trajectory analysis (Figure 8b) which showed air masses arriving at the Bodega Bay site coming directly from the ocean (green lines), aerosol composition during the AR event measured by the ATOFMS indicated a predominance of marine aerosol (Figure 7). Spatially, as shown in Figure 9, marine aerosol was dominant in clouds over the ocean and along the shore, with a small increase in local pollution aerosol as the storm, and flight tracks, moved inland across Sacramento and into the mountains. Further, airborne measurements of aerosol composition showed almost no dust or biological particles, the influence of which as INPs would also clearly be reflected in the n_s results (Cornwell, 2019). Congruent with the dominance of marine aerosol during the AR event, we found that n_s values measured aboard the G-1, in clear air, as well as from IS data from the Ronald H. Brown agreed well with measurements made in both laboratory and ambient settings of marine aerosol, shown in Figure 10. Nearly all n_s values measured during the AR fell within the range of previously measured marine INP data and were well below values that would suggest major dust influence. The one notable outlier to this trend was at the colder end of the Bodega Bay IS measurement spectrum where n_s values measured during the AR event trended toward higher values, and above the range of marine values. This departure from the clean marine fit line indicates that other, more active INP types were contributing to the INP population at these colder temperatures during this time period. Cornwell (2019) used a CFDC and ATOFMS connected in series with a pumped counterflow virtual impactor to measure the chemical composition of activated INPs at the Bodega Bay surface site. They found that while sea salt was the dominant component of the ambient aerosol, dust particles were still the

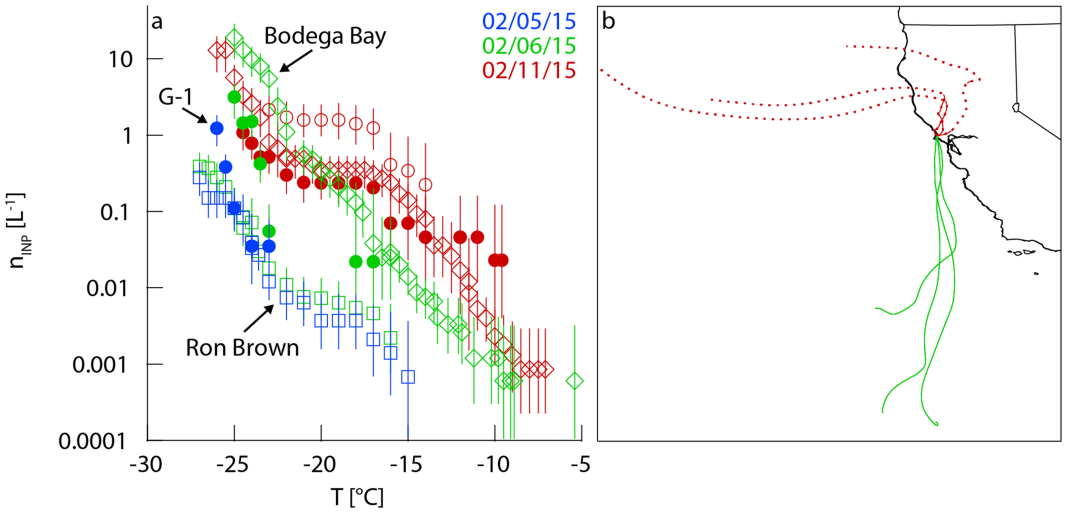

Figure 8. (a) n_{INP} as the AR approached land (blue), made landfall (green), and after the event (red) measured by IS filters from the Ronald H. Brown (squares), the Bodega Bay surface site (diamonds), and the G-1 (circles). (b) The 48-hr back trajectories using the Hybrid Single-Particle Lagrangian Integrated Trajectory (HYSPLIT; Draxler & Hess, 1998) and the Global Data Assimilation System (GDAS) one-degree meteorological data set. Solid lines show times when the trajectory height was below 1,000 m, and dotted lines when it was above this level. Colors indicate the same dates as in (a).

predominant contributor to the INP population at −30 °C. While these measurements were made after the AR time period (from 12–19 February), they also saw a consistent contribution of dust aerosol from ATOFMS measurements during the entire ACAPEX time period (Cornwell, 2019) and this likely accounts for the higher n_s values measured at colder temperatures at this site. From the G-1 data, however, the majority of calculated n_s values fell within the clean marine range. Further, unlike the surface site, dust was not a significant contributor in the airborne ATOFMS measurements. Thus, local sources and not long-range transport associated with the AR could account for the increased n_s values measured at the surface site during this time period. Although the presence of a few dust particles, even at levels below the detection limit of the ATOFMS, could be contributing to the INP population, the generally low n_s values calculated from airborne measurements suggests that marine aerosols were a dominant contributor both to bulk aerosol composition and the INP population for these airborne measurements.

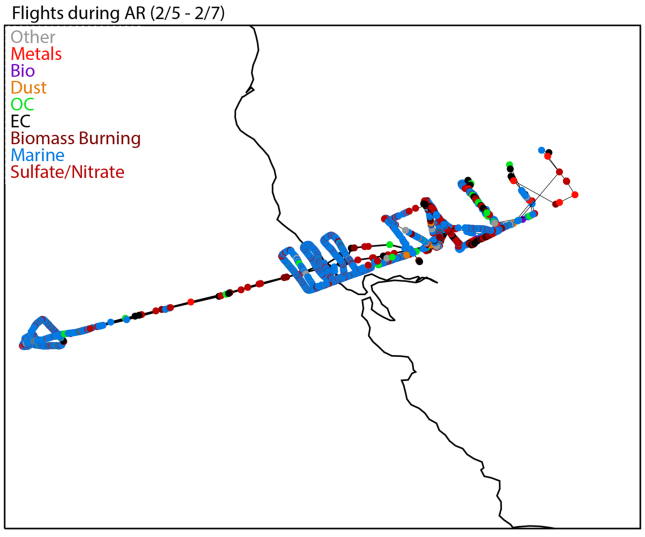

Figure 9. Spatial distribution of aerosol composition during the AR flights (5–7 February) measured by the ATOFMS aboard the G-1. Points show individual ATOFMS measurements colored by particle classification (Table 1).

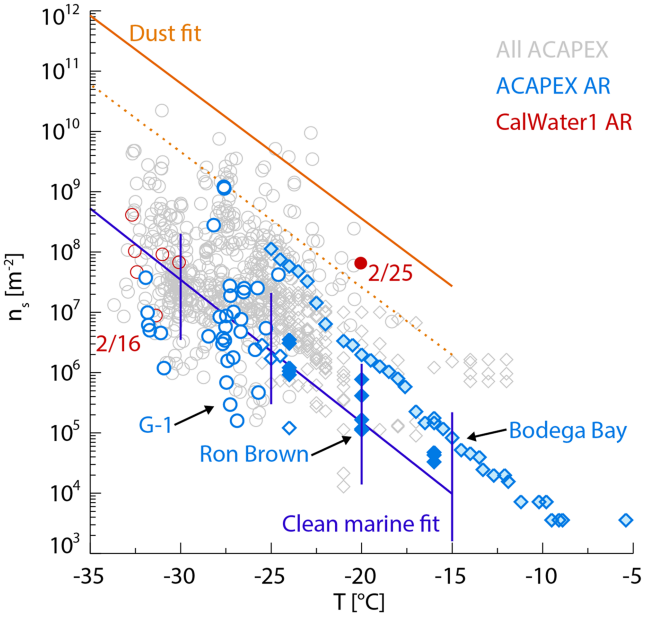

Figure 10. All n_s values measured during ACAPEX (grey) with values measured during the AR event, 5–7 February 2015, from the CFDC onboard the G-1, and from filter measurements on the Ronald H. Brown research vessel and at the Bodega Bay surface site all highlighted in blue and labeled. Circles indicate CFDC measurements, diamonds show IS filter measurements, and symbol fill is site specific (white for G-1, light blue for Bodega Bay, and dark blue for the Ronald H. Brown). Values from two AR events measured in clear air regions with the CFDC on the G-1 during CalWater-1 on 16 February 2011 (open circles) and 25 February 2011 (filled circle) are shown in red and labeled with the dates. Note that the aircraft measurements were only from times when we were flying in clear air above or below clouds. Orange and purple lines are the same as in Figure 6.

While marine aerosol were dominant during the AR event, one specific cluster type measured by the ATOFMS, cluster #1 in Table 1, accounted for almost all of the marine aerosol during this time period. This cluster was identified as containing a mixture of sea salt and high molecular weight organic oligomers. Measurements corresponding to these clusters, as well as other marine aerosol, are highlighted in Figure 11. While most of the n_s values associated with marine aerosol clusters fell within the range of previous marine INP measurements, some of them were higher, even close to the dust parameterization. By contrast, the n_s values associated with Cluster #1 agree very well with the other n_s values measured for known marine INPs.

Previous studies, using the same instrumentation, have suggested that dust aerosol transported with ARs is a major source of INPs during these events (Ault et al., 2011; Creamean et al., 2013). During the 2011 CalWater-1 campaign, ATOFMS measurements made during an AR event on 16 February showed that 50% of the particles from CVI measurements of cloud residuals in clouds over the Sierra Nevada range were dust (Creamean et al., 2013; Creamean et al., 2015). It was inferred that this dust was likely coming in distinct layers that were seeding the tops of clouds, while lower clouds were deeply supercooled and of marine air origin. Measurements from clear-air regions on the same flight, mostly at lower altitudes, showed very little dust during this event, with the majority of aerosol being composed of sea salt, but notably not the marine organic aerosol observed during the 2015 AR event. When comparing the n_s values from this time period, again for clear air measurements only, the values fall in line with the n_s values for other marine aerosol dominated measurements (Figure 10). By contrast to this, on 25 February 2011, airborne ATOFMS measurements made during another AR event showed that dust mixed with biological particles were a dominant aerosol type in both clear air and cloud residual measurements. While we were only able to calculate an n_s value during one CFDC sample period for this case, the value falls in line with other CFDC dust measurements, highlighted in Figure 10.

Unlike during periods of CalWater-1, the clear air and in-cloud ATOFMS data, as well as n_s values calculated from airborne clear air measurements during ACAPEX indicated that dust was not a dominant INP type. However, we cannot completely rule dust out as a potential INP type during the ACAPEX AR event, as

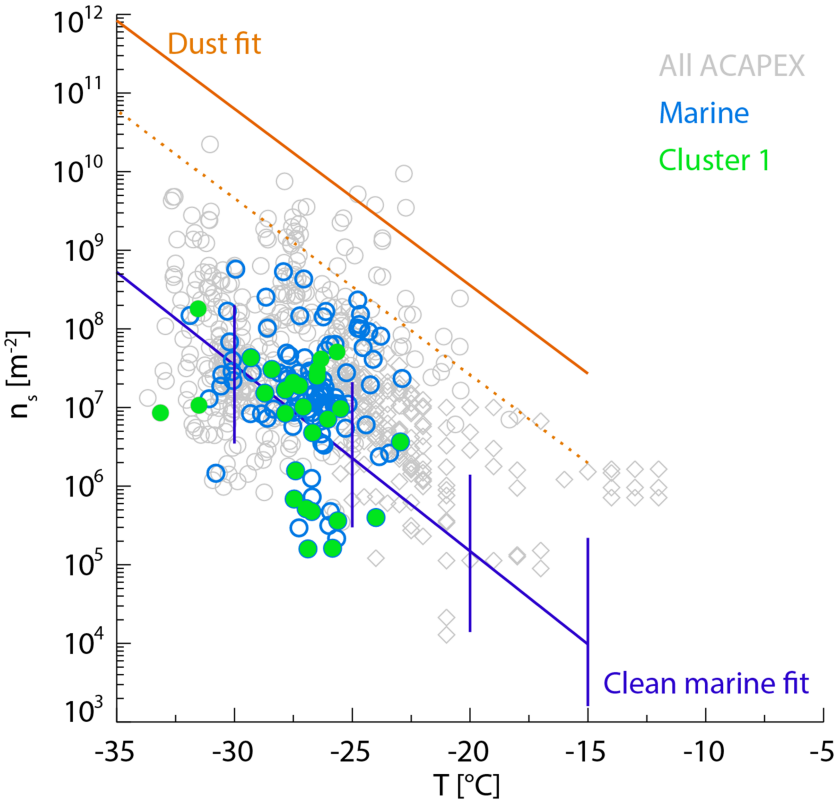

Figure 11. n_s values measured by the CFDC (circles) and IS (diamonds) from the G-1 during ACAPEX (grey). Values measured when the ATOFMS detected any marine aerosol particles are shown in blue and those when the ATOFMS detected Cluster 1 (sea salt + HMOC) are highlighted in green. Orange and purple lines are the same as in Figure 6.

even a very small number of dust particles could account for the majority of INPs. Figure 12 shows timelines of aerosol $PM_{2.5}$ composition measured by the IMPROVE samplers at Point Reyes, Bliss State Park, and Yellowstone National Park (locations shown in Figure 1). Both total mass and mass fractions are shown for the five common aerosol components routinely measured by the IMPROVE network. For the Point Reyes station, the site closest to the Bodega Bay surface site, we also show a historical average, representing data averaged over the ACAPEX sampling period (16 January to 7 March) for the entire IMPROVE data record for this site (1988 to 2015). As can be seen in Figure 12, as the AR was approaching land on 5 February there was an increase in sea salt measured at Point Reyes with a large increase observed on 8 February. Since the IMPROVE network only samples every third day, there were no measurements between these two samples. This increase in sea salt concentrations at the coast was consistent with the sea salt measured by the ATOFMS near Bodega Bay on 5–8 February. In the mountains, however, ahead of the AR event on 5 February, there was an increase in the mass fraction of soil, or dust, in the sampled aerosol. Although the total concentrations were low, ~0.5 μg/m^3, this represented more than a doubling of the soil mass from the previous measurement at both sites. Because this increase in soil components was seen only at higher elevations, and not at the coast, it could indicate a transient elevated dust layer that was associated with the AR. However, this dust layer was not observed by the airborne measurements, even when transiting at high altitude (~5,000 m) out to the leading edge of the AR on the 5 February or when flying above the Sierra Nevada range on 6 and 7 February. Further, no dust particles were measured in cloud residuals when measuring with ATOFMS from the CVI inlet during the storm. It should also be noted that the large increase in sea salt mass fraction at Point Reyes during the AR event was anomalous when compared to the historical average for that site during that time of year, highlighting both the episodic and variable nature of these types of events. While there was very little increase in sea salt aerosol mass observed at the higher-elevation sites, measurements were not made at these sites on 6 or 7 February, as the storm was moving into the mountains. Further, previous studies

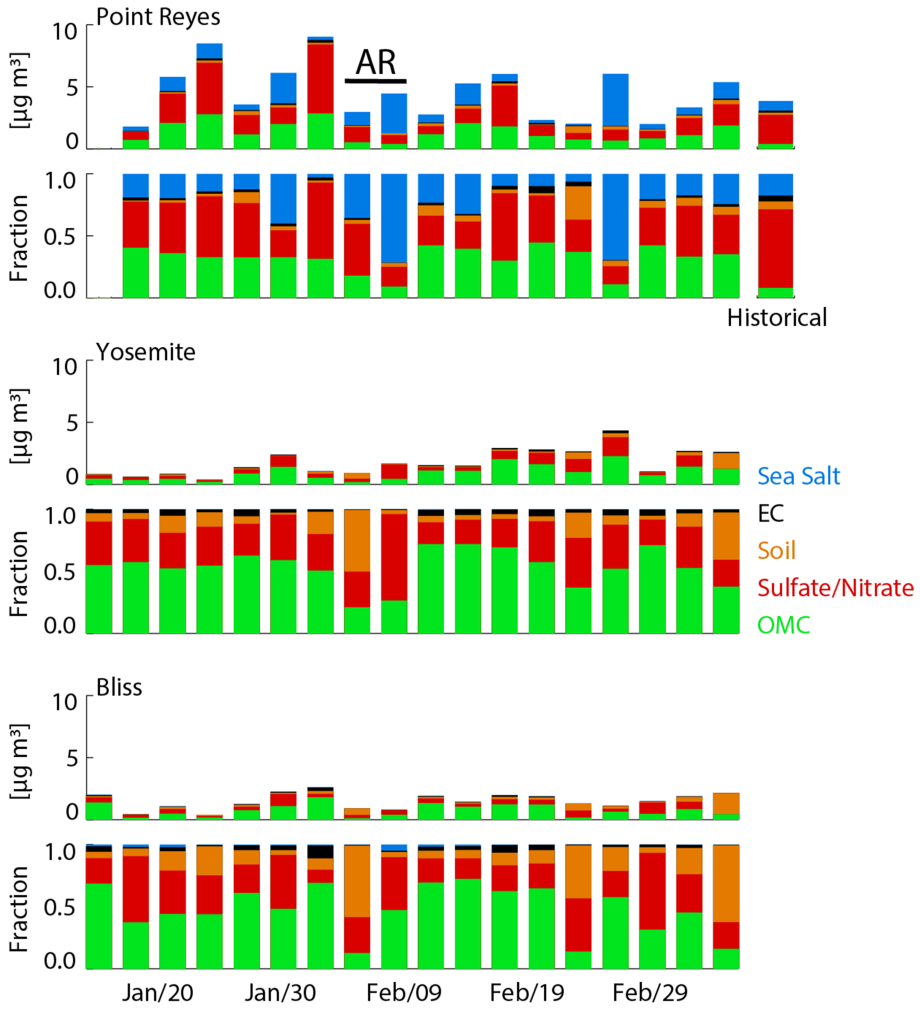

Figure 12. The 24-hr $PM_{2.5}$ composition data from IMPROVE network samplers measured every third day at Point Reyes (lat = 38.1224, lon = −122.9085, alt = 97 m asl), Yosemite National Park (lat = 37.7133, lon = −119.7061, alt = 1,603 m asl) and Bliss State Park (lat = 38.9761, lon = −120.1024, alt = 2,130.67 m asl) for the entire ACAPEX measurement period.

have shown that low-level flow (the Sierra barrier jet) often blocks marine air masses from reaching the surface at these higher elevations (Ralph et al., 2016).

4. Conclusions

As part of ACAPEX we collected real-time and filter-based measurements of INPs throughout central California during the winter of 2015, creating an extensive data set of INP number across a large temperature range. Over the entire ACAPEX study period, real-time INP number concentrations (n_{INP}) measured with the CSU-CFDC at processing temperatures between −20 and −30 °C ranged from <1 to 10s L^{-1}. Filter measurements processed in the CSU Ice Spectrometer extended the INP measurement range to −10 °C, detecting n_{INP} as low as ~0.01 L^{-1}. Good agreement was observed between both of the INP measurements in the overlapping temperature region. CFDC measurements made during ACAPEX also agreed well with data collected from the same instrument and aircraft during the 2011 CalWater measurement campaign with similar n_{INP} values at the same processing temperatures between the two studies. During ACAPEX, there was considerable scatter in n_{INP} as well as INP normalized by total aerosol concentration (ξ_T) and aerosol surface area (n_s), indicating changes in both n_{INP} and INP composition over the study period. Vertically, although there was large

variability within each layer, we did observe an increase in ξ_T values with altitude, likely indicating that the higher concentration of pollution aerosols near the surface were poor sources of INPs.

During ACAPEX, pollution aerosol (particles containing sulfate and nitrate) and marine aerosol each comprised about one third of the particles measured by the airborne ATOFMS, with biomass burning particles and EC comprising much of the remainder. However, there was a distinct difference in aerosol composition between flights. Sulfate, nitrate, EC, and biomass burning particles were dominant during clear air flights, especially when measuring in the southern Central Valley, while marine aerosol was the dominant aerosol component in marine cloud residuals. Dust and biological particles which have been previously associated as INPs in wintertime precipitation events in California (Creamean et al., 2013) were only very minor contributors to the measured aerosol population over the course of the campaign. However, even a small number of these efficient ice nucleators can account for the majority of INPs (Cornwell, 2019). Measurements of INP surface site density (n_s) was used to investigate the relative contribution of certain INP types by comparison to n_s parameterizations for dust aerosol (Niemand et al., 2012; Ullrich et al., 2017) and clean marine INP (McCluskey, et al., 2018). During ACAPEX, n_s values largely fell between these two bounding parameterizations, although with more values in the region of clean marine INPs. However, any n_s value above the range of clean marine values indicates some contribution from more active INP types, such as dust and/or terrestrial biological INPs, even if the number concentrations of these particles were too low to measure with the ATOFMS.

A main purpose of ACAPEX, and the broader CalWater campaign, was to improve our understanding of ARs, and the storms associated with them, which are crucial for water budgets in California and throughout the western United States. During ACAPEX, we sampled one major landfalling AR event from 5–7 February 2015. Airborne measurements of single-particle aerosol composition were dominated by marine aerosol, especially over the ocean and near the coast, with anthropogenic pollution particles contributing a relatively small amount as the storm moved inland. Dust and biological particles were almost completely absent in the ATOFMS measurements during the AR event. Congruent with the measured aerosol composition, n_s values calculated during the AR event were much closer to previous measurements of sea spray INP than dust, although IS measurements at the surface site in Bodega Bay did indicate some higher n_s values at colder temperatures. Increases in biological INPs appeared to ensue following the AR event and additional studies are needed to assess if terrestrial biological INP production is a common feature following winter rainfall events at lower elevations, and to improve understanding and predictability of their populations.

Previous studies of residual particles in precipitation from California winter storms have shown that dust and biological particles are important for ice nucleation, with the specific aerosol type changing from one storm to another (Ault et al., 2011; Creamean et al., 2013; Creamean et al., 2014; Creamean et al., 2015). Further, the type of INPs present can have large impacts on precipitation timing and amount and the extent of supercooling within a cloud (Fan et al., 2014; Fan et al., 2017; Rosenfeld et al., 2013). Here we present the possibility that marine INPs can sometimes dominate INP populations influencing winter storms and provide a general baseline of INP activity for air lofted over the Sierra Nevada range. As reported by DeMott et al. (2016), marine INPs are distinctly different from other common INP types, with much lower values of n_s, compared with dust aerosol, for example. However, in the absence of these other, more active, INP types, and given the relatively large concentrations of marine aerosol generated by landfalling storms, these particles could play an important role in ice production associated with AR events along the western United States. At the least, there is no requirement for dust particles for efficient precipitation processes to occur. A major conclusion of this work, therefore, is that not all AR events are the same. While previous studies have shown that an elevated dust layer can lead to a "seeder-feeder" type mechanism within a landfalling AR, the source region and transport pathways of enhanced water vapor and dust aerosol are separate and, thus, these episodic events might not always co-occur. This work strongly suggests that future modeling studies should incorporate marine sea spray aerosols and mineral/soil dust particles and their associated but unique INPs explicitly in studies of aerosol impacts on precipitation along the west coast of the United States, and perhaps in general.

A natural extension of the present studies will be to examine the INP fields in comparison to the development of ice crystal concentrations and precipitation in these winter storms. Combining analysis of the measurements and modeling will be useful to understand the impacts of the marine INPs on precipitation during the ACAPEX AR event.

Acknowledgments
This research was supported primarily by the U.S. Department of Energy's Atmospheric System Research, an Office of Science, Office of Biological and Environmental Research program, under grant DE-SC0014354. Funding for installation and data collection on the AAF G-1 aircraft and onboard the NOAA R/V *Ronald H. Brown* was supported by the Atmospheric Radiation Measurement (ARM) user facility, a U.S. Department of Energy (DOE) Office of Science user facility managed by the Office of Biological and Environmental Research. The deployment of the G-1 also involved the assistance of many PNNL/Atmospheric Radiation Measurement field staff during both CalWater-2011 and ACAPEX, including E. Dukes, C. Kluzek, H. Jonsson, and B. Schmid. M. Hubbell and B. Svancara flew the G-1 for the CalWater-2011 flight campaign, and M. Hubbell and C. Eveland flew the G-1 during ACAPEX. We also thank Michael Ritsche, Amon Haruta, Pat Dowell, and Mark Smith for the shipment coordination and technical support on the Ronald H. Brown. Partial support for this research was provided by NSF award AGS-1451347 (H.A.-M., G.C.C., L.J.K., K.A.P.) and NSF award 1450760 (E.J.T.L., S.M.K., P. J.D., K.J.S., C.S.M.). Funding for the Calwater-2011 study was provided by the California Energy Commission under contract CEC 500-09-043. G.P.S. acknowledges support from an NSF Postdoctoral Fellowship (award 1433517). Y.B. was supported by a doctoral exchange grant by the Zeno Karl Schindler foundation. The authors would also like to thank the UC Davis Bodega Marine Laboratory for the use of laboratory and office space, and shipping and physical plant support while collecting data at the Bodega Bay site, as well as the California Air Resources Board and the National Park Service for the trailers used for sampling. IMPROVE is a collaborative association of state, tribal, and federal agencies, and international partners. U. S. Environmental Protection Agency is the primary funding source, with contracting and research support from the National Park Service. The Air Quality Group at the University of California, Davis is the central analytical laboratory, with ion analysis provided by Research Triangle Institute, and carbon analysis provided by Desert Research Institute. We acknowledge the use of imagery from the NASA Worldview application (https://worldview.earthdata.nasa.gov), part of the NASA Earth Observing System Data and Information System (EOSDIS). All data from ACAPEX are available at

References

Ault, A. P., Williams, C. R., White, A. B., Neiman, P. J., Creamean, J. M., Gaston, C. J., et al. (2011). Detection of Asian dust in California orographic precipitation. *Journal of Geophysical Research*, *116*, D16205. https://doi.org/10.1029/2010jd015351

Agresti, A., & Coull, B. A. (1998). pproximate is betterthan "exact" for interval estimation of binomial proportions A. *American Statistician*, *52*(2), 119–126. https://doi.org/10.2307/2685469

Boose, Y., Sierau, B., Garcia, M. I., Rodriguez, S., Alastuey, A., Linke, C., et al. (2016). Ice nucleating particles in the Saharan Air Layer. *Atmospheric Chemistry and Physics*, *16*(14), 9067–9087. https://doi.org/10.5194/acp-16-9067-2016

Chen, J., Wu, Z. J., Augustin-Bauditz, S., Grawe, S., Hartmann, M., Pei, X. Y., et al. (2018). Ice-nucleating particle concentrations unaffected by urban air pollution in Beijing, China. *Atmospheric Chemistry and Physics*, *18*(5), 3523–3539. https://doi.org/10.5194/acp-18-3523-2018

Choularton, T. W., & Perry, S. J. (1986). A Model of the Orographic Enhancement of Snowfall by the Seeder-Feeder Mechanism. *Quarterly Journal of the Royal Meteorological Society*, *112*(472), 335–345. https://doi.org/10.1256/smsqj.47203

Cordeira, J. M., Ralph, F. M., Martin, A., Gaggggini, N., Spackman, J. R., Neiman, P. J., et al. (2017). Forecasting Atmospheric Rivers during CalWater 2015. *Bulletin of the American Meteorological Society*, *98*(3), 449–459. https://doi.org/10.1175/bams-d-15-00245.1

Cornwell, G. C. (2019). *Investigating the impacts of aerosols upon coastal clouds*. San Diego, San Diego, CA, USA: University of California.

Creamean, J. M., Ault, A. P., White, A. B., Neiman, P. J., Ralph, F. M., Minnis, P., & Prather, K. A. (2015). Impact of interannual variations in sources of insoluble aerosol species on orographic precipitation over California's central Sierra Nevada. *Atmospheric Chemistry and Physics*, *15*(11), 6535–6548. https://doi.org/10.5194/acp-15-6535-2015

Creamean, J. M., Lee, C., Hill, T. C., Ault, A. P., DeMott, P. J., White, A. B., et al. (2014). Chemical properties of insoluble precipitation residue particles. *Journal of Aerosol Science*, *76*, 13–27. https://doi.org/10.1016/j.jaerosci.2014.05.005

Creamean, J. M., Suski, K. J., Rosenfeld, D., Cazorla, A., DeMott, P., Sullivan, R. C., et al. (2013). Dust and Biological Aerosols from the Sahara and Asia Influence Precipitation in the Western U. S. *Science*, *339*(6127), 1572–1578. https://doi.org/10.1126/science.1227279

DeBell, L. J., K. A. Gebhart, J. L. Hand, W. C. Malm, M. L. Pitchford, B. A. Schichtel, and W. H. White (2006), Spatial and seasonal patterns and temporal variability of haze and its constituents in the United States*Rep*. Report IV, Cooperative Institute for Research in the Atmosphere, Fort Collins, CO.

DeMott, P. J., Hill, T. C. J., McCluskey, C. S., Prather, K. A., Collins, D. B., Sullivan, R. C., et al. (2016). Sea spray aerosol as a unique source of ice nucleating particles. *Proceedings of the National Academy of Sciences of the United States of America*, *113*(21), 5797–5803. https://doi.org/10.1073/pnas.1514034112

DeMott, P. J., Hill, T. C. J., Petters, M. D., Bertram, A. K., Tobo, Y., Mason, R. H., et al. (2017). Comparative measurements of ambient atmospheric concentrations of ice nucleating particles using multiple immersion freezing methods and a continuous flow diffusion chamber. *Atmospheric Chemistry and Physics*, *17*(18), 11,227–11,245. https://doi.org/10.5194/acp-17-11227-2017

DeMott, P. J., Prenni, A. J., Liu, X., Kreidenweis, S. M., Petters, M. D., Twohy, C. H., et al. (2010). Predicting global atmospheric ice nuclei distributions and their impacts on climate. *Proceedings of the National Academy of Sciences of the United States of America*, *107*(25), 11217–11222. https://doi.org/10.1073/pnas.0910818107

DeMott, P. J., Prenni, A. J., McMeeking, G. R., Sullivan, R. C., Petters, M. D., Tobo, Y., et al. (2015). Integrating laboratory and field data to quantify the immersion freezing ice nucleation activity of mineral dust particles. *Atmospheric Chemistry and Physics*, *15*(1), 393–409. https://doi.org/10.5194/acp-15-393-2015

Dettinger, M. D., Ralph, F. M., Das, T., Neiman, P. J., & Cayan, D. R. (2011). Atmospheric Rivers, Floods and the Water Resources of California. *Water*, *3*(2), 445–478. https://doi.org/10.3390/w3020445

Draxler, R. R., & Hess, G. D. (1998). An overview of the HYSPLIT_4 modelling system for trajectories, dispersion and deposition. *Australian Meteorological Magazine*, *47*(4), 295–308.

Eidhammer, T., DeMott, P. J., Prenni, A. J., Petters, M. D., Twohy, C. H., Rogers, D. C., et al. (2010). Ice Initiation by Aerosol Particles: Measured and Predicted Ice Nuclei Concentrations versus Measured Ice Crystal Concentrations in an Orographic Wave Cloud. *Journal of the Atmospheric Sciences*, *67*(8), 2417–2436. https://doi.org/10.1175/2010jas3266.1

Fan, J., Leung, L. R., DeMott, P. J., Comstock, J. M., Singh, B., Rosenfeld, D., et al. (2014). Aerosol impacts on California winter clouds and precipitation during CalWater 2011: Local pollution versus long-range transported dust. *Atmospheric Chemistry and Physics*, *14*(1), 81–101. https://doi.org/10.5194/acp-14-81-2014

Fan, J., Leung, L. R., Rosenfeld, D., & DeMott, P. J. (2017). Effects of cloud condensation nuclei and ice nucleating particles on precipitation processes and supercooled liquid in mixed-phase orographic clouds. *Atmospheric Chemistry and Physics*, *17*(2), 1017–1035. https://doi.org/10.5194/acp-17-1017-2017

Hallett, J., & Mossop, S. C. (1974). Production of Secondary Ice Particles During Riming Process. *Nature*, *249*(5452), 26–28. https://doi.org/10.1038/249026a0

Hill, T. C. J., DeMott, P. J., Tobo, Y., Froehlich-Nowoisky, J., Moffett, B. F., Franc, G. D., & Kreidenweis, S. M. (2016). Sources of organic ice nucleating particles in soils. *Atmospheric Chemistry and Physics*, *16*(11), 7195–7211. https://doi.org/10.5194/acp-16-7195-2016

Hill, T. C. J., McCluskey, C., Michaud, J., Santander, M., Cornwell, G., Sultana, C., et al. (2016). *Characteristics of ice nucleating particles in seawater and sea spray aerosol produced during laboratory phytoplankton blooms, Abstracts of Papers of the American Chemical Society*, (Vol. *251*). Washington, Dc: American Chemical Society.

Hirano, S. S., Baker, L. S., & Upper, C. D. (1996). Raindrop momentum triggers growth of leaf-associated populations of Pseudomonas syringae on field-grown snap bean plants. *Applied and Environmental Microbiology*, *62*(7), 2560–2566.

Hiranuma, N., Augustin-Bauditz, S., Bingemer, H., Budke, C., Curtius, J., Danielczok, A., et al. (2015). A comprehensive laboratory study on the immersion freezing behavior of illite NX particles: A comparison of 17 ice nucleation measurement techniques. *Atmospheric Chemistry and Physics*, *15*(5), 2489–2518. https://doi.org/10.5194/acp-15-2489-2015

Hoose, C., & Moehler, O. (2012). Heterogeneous ice nucleation on atmospheric aerosols: A review of results from laboratory experiments. *Atmospheric Chemistry and Physics*, *12*(20), 9817–9854. https://doi.org/10.5194/acp-12-9817-2012

Huffman, J. A., Prenni, A. J., DeMott, P. J., Pöhlker, C., Mason, R. H., Robinson, N. H., et al. (2013). High concentrations of biological aerosol particles and ice nuclei during and after rain. *Atmospheric Chemistry and Physics*, *13*(13), 6151–6164. https://doi.org/10.5194/acp-13-6151-2013

Kim, J., Guan, B., Waliser, D. E., Ferraro, R. D., Case, J. L., Iguchi, T., et al. (2018). Winter precipitation characteristics in western US related to atmospheric river landfalls: Observations and model evaluations. *Climate Dynamics*, *50*(1-2), 231–248. https://doi.org/10.1007/s00382-017-3601-5

https://www.arm.gov/research/campaigns/amf2015apex and from CalWater 2011 at https://www.arm.gov/research/campaigns/aaf2011calwater.

Kupc, A., Williamson, C., Wagner, N. L., Richardson, M., & Brock, C. A. (2018). Modification, calibration, and performance of the Ultra-High Sensitivity Aerosol Spectrometer for particle size distribution and volatility measurements during the Atmospheric Tomography Mission (ATom) airborne campaign. *Atmospheric Measurement Techniques*, *11*(1), 369–383. https://doi.org/10.5194/amt-11-369-2018

Lacher, L., DeMott, P. J., Levin, E. J. T., Suski, K. J., Boose, Y., Zipori, A., et al. (2018). Background Free-Tropospheric Ice Nucleating Particle Concentrations at Mixed-Phase Cloud Conditions. *Journal of Geophysical Research: Atmospheres*, *123*, 10,506–510,525. https://doi.org/10.1029/2018JD028338

Lauber, A., Kiselev, A., Pander, T., Handmann, P., & Leisner, T. (2018). Secondary Ice Formation during Freezing of Levitated Droplet. *Journal of the Atmospheric Sciences*, *75*(8), 2815–2826. https://doi.org/10.1175/jas-d-18-0052.1

Levin, E. J. T., McMeeking, G. R., DeMott, P. J., McCluskey, C. S., Carrico, C. M., Nakao, S., et al. (2016). Ice-nucleating particle emissions from biomass combustion and the potential importance of soot aerosol. *Journal of Geophysical Research: Atmospheres*, *121*, 5888–5903. https://doi.org/10.1002/2016jd024879

Malm, W. C., Schichtel, B. A., Pitchford, M. L., Ashbaugh, L. L., & Eldred, R. A. (2004). Spatial and monthly trends in speciated fine particle concentration in the United States. *Journal of Geophysical Research*, *109*, D03306. https://doi.org/10.1029/2003jd003739

Martin, A. C., Cornwell, G., Beall, C. M., Cannon, F., Reilly, S., Schaap, B., et al. (2019). Contrasting local and long-range-transported warm ice-nucleating particles during an atmospheric river in coastal California, USA. *Atmospheric Chemistry and Physics*, *19*(7), 4193–4210. https://doi.org/10.5194/acp-19-4193-2019

Martin, A. C., Cornwell, G. C., Atwood, S. A., Moore, K. A., Rothfuss, N. E., Taylor, H., et al. (2017). Transport of pollution to a remote coastal site during gap flow from California's interior: Impacts on aerosol composition, clouds, and radiative balance. *Atmospheric Chemistry and Physics*, *17*(2), 1491–1509. https://doi.org/10.5194/acp-17-1491-2017

Martin, A. C., et al. (2019). Contrasting local andlong-range-transported warm ice-nucleating particles during an atmosphericriver in coastal California, USA. *AtmosphericChemistry and Physics*, 4193–4210. *19*(7). https://doi.org/10.5194/acp-19-4193-2019 McCluskey, C. S., DeMott, P. J., Prenni, A. J., Levin, E. J. T., McMeeking, G. R., Sullivan, A. P., et al. (2014). Characteristics of atmospheric ice nucleating particles associated with biomass burning in the US: Prescribed burns and wildfires. *Journal of Geophysical Research: Atmospheres*, *119*, 10458–10470. https://doi.org/10.1002/2014jd021980

McCluskey, C. S., Hill, T. C. J., Malfatti, F., Sultana, C. M., Lee, C., Santander, M. V., et al. (2017). A Dynamic Link between Ice Nucleating Particles Released in Nascent Sea Spray Aerosol and Oceanic Biological Activity during Two Mesocosm Experiments. *Journal of the Atmospheric Sciences*, *74*(1), 151–166. https://doi.org/10.1175/jas-d-16-0087.1

McCluskey, C. S., Hill, T. C. J., Sultana, C. M., Laskina, O., Trueblood, J., Santander, M. V., et al. (2018). A Mesocosm Double Feature: Insights into the Chemical Makeup of Marine Ice Nucleating Particles. *Journal of the Atmospheric Sciences*, *75*(7), 2405–2423. https://doi.org/10.1175/jas-d-17-0155.1

McCluskey, C. S., Ovadnevaite, J., Rinaldi, M., Atkinson, J., Belosi, F., Ceburnis, D., et al. (2018). Marine and Terrestrial Organic Ice-Nucleating Particles in Pristine Marine to Continentally Influenced Northeast Atlantic Air Masses. *Journal of Geophysical Research: Atmospheres*, *123*, 6196–6212. https://doi.org/10.1029/2017jd028033

Murray, B. J., O'Sullivan, D., Atkinson, J. D., & Webb, M. E. (2012). Ice nucleation by particles immersed in supercooled cloud droplets. *Chemical Society Reviews*, *41*(19), 6519–6554. https://doi.org/10.1039/c2cs35200a

Niemand, M., Möhler, O., Vogel, B., Vogel, H., Hoose, C., Connolly, P., et al. (2012). A Particle-Surface-Area-Based Parameterization of Immersion Freezing on Desert Dust Particles. *Journal of the Atmospheric Sciences*, *69*(10), 3077–3092. https://doi.org/10.1175/jas-d-11-0249.1

Petters, M. D., & Kreidenweis, S. M. (2007). A single parameter representation of hygroscopic growth and cloud condensation nucleus activity. *Atmospheric Chemistry and Physics*, *7*(8), 1961–1971.

Petters, M. D., Parsons, M. T., Prenni, A. J., DeMott, P. J., Kreidenweis, S. M., Carrico, C. M., et al. (2009). Ice nuclei emissions from biomass burning. *Journal of Geophysical Research*, *114*, D07209. https://doi.org/10.1029/2008jd011532

Petters, M. D., & Wright, T. P. (2015). Revisiting ice nucleation from precipitation samples. *Geophysical Research Letters*, *42*, 8758–8766. https://doi.org/10.1002/2015gl065733

Pratt, K. A., Mayer, J. E., Holecek, J. C., Moffet, R. C., Sanchez, R. O., Rebotier, T. P., et al. (2009). Development and Characterization of an Aircraft Aerosol Time-of-Flight Mass Spectrometer. *Analytical Chemistry*, *81*(5), 1792–1800. https://doi.org/10.1021/ac801942r

Prenni, A. J., Tobo, Y., Garcia, E., DeMott, P. J., Huffman, J. A., McCluskey, C. S., et al. (2013). The impact of rain on ice nuclei populations at a forested site in Colorado. *Geophysical Research Letters*, *40*, 227–231. https://doi.org/10.1029/2012gl053953

Ralph, F. M., Coleman, T., Neiman, P. J., Zamora, R. J., & Dettinger, M. D. (2013). Observed Impacts of Duration and Seasonality of Atmospheric-River Landfalls on Soil Moisture and Runoff in Coastal Northern California. *Journal of Hydrometeorology*, *14*(2), 443–459. https://doi.org/10.1175/jhm-d-12-076.1

Ralph, F. M., Cordeira, J. M., Neiman, P. J., & Hughes, M. (2016). Landfalling Atmospheric Rivers, the Sierra Barrier Jet, and Extreme Daily Precipitation in Northern California's Upper Sacramento River Watershed. *Journal of Hydrometeorology*, *17*(7), 1905–1914. https://doi.org/10.1175/jhm-d-15-0167.1

Ralph, F. M., Iacobellis, S. F., Neiman, P. J., Cordeira, J. M., Spackman, J. R., Waliser, D. E., et al. (2017). Dropsonde Observations of Total Integrated Water Vapor Transport within North Pacific Atmospheric Rivers. *Journal of Hydrometeorology*, *18*(9), 2577–2596. https://doi.org/10.1175/jhm-d-17-0036.1

Ralph, F. M., Prather, K. A., Cayan, D., Spackman, J. R., DeMott, P., Dettinger, M., et al. (2016). Calwater Field Studies Designed To Quantify The Roles Of Atmospheric Rivers And Aerosols In Modulating Us West Coast Precipitation In A Changing Climate. *Bulletin of the American Meteorological Society*, *97*(7), 1209–1228. https://doi.org/10.1175/bams-d-14-00043.1

Rebotier, T. P., & Prather, K. A. (2007). Aerosol time-of-flight mass spectrometry data analysis: A benchmark of clustering algorithms. *Analytica Chimica Acta*, *585*(1), 38–54. https://doi.org/10.1016/j.aca.2006.12.009

Rogers, D. C., DeMott, P. J., Kreidenweis, S. M., & Chen, Y. L. (2001). A continuous-flow diffusion chamber for airborne measurements of ice nuclei. *Journal of Atmospheric and Oceanic Technology*, *18*(5), 725–741. https://doi.org/10.1175/1520-0426(2001)018<0725:acfdcf>2.0.co;2

Rosenfeld, D., Chemke, R., DeMott, P., Sullivan, R. C., Rasmussen, R., McDonough, F., et al. (2013). The common occurrence of highly supercooled drizzle and rain near the coastal regions of the western United States. *Journal of Geophysical Research: Atmospheres*, *118*, 9819–9833. https://doi.org/10.1002/jgrd.50529

Rosenfeld, D., Chemke, R., Prather, K., Suski, K., Comstock, J. M., Schmid, B., et al. (2014). Polluting of winter convective clouds upon transition from ocean inland over central California: Contrasting case studies. *Atmospheric Research*, *135*, 112–127. https://doi.org/10.1016/j.atmosres.2013.09.006

Schill, G. P., Jathar, S. H., Kodros, J. K., Levin, E. J. T., Galang, A. M., Friedman, B., et al. (2016). Ice-nucleating particle emissions from photochemically aged diesel and biodiesel exhaust. *Geophysical Research Letters*, *43*, 5524–5531. https://doi.org/10.1002/2016gl069529

Schmid, B., Tomlinson, J. M., Hubbe, J. M., Comstock, J. M., Mei, F., Chand, D., et al. (2014). The Doe Arm Aerial Facility. *Bulletin of the American Meteorological Society*, *95*(5), 723–742. https://doi.org/10.1175/bams-d-13-00040.1

Song, X. H., Hopke, P. K., Fergenson, D. P., & Prather, K. A. (1999). Classification of single particles analyzed by ATOFMS using an artificial neural network, ART-2A. *Analytical Chemistry*, *71*(4), 860–865. https://doi.org/10.1021/ac9809682

Stith, J. L., Twohy, C. H., DeMott, P. J., Baumgardner, D., Campos, T., Gao, R., & Anderson, J. (2011). Observations of ice nuclei and heterogeneous freezing in a Western Pacific extratropical storm. *Atmospheric Chemistry and Physics*, *11*(13), 6229–6243. https://doi.org/10.5194/acp-11-6229-2011

Sultana, C. M., Cornwell, G. C., Rodriguez, P., & Prather, K. A. (2017). FATES: A flexible analysis toolkit for the exploration of single-particle mass spectrometer data. *Atmospheric Measurement Techniques*, *10*(4), 1323–1334. https://doi.org/10.5194/amt-10-1323-2017

Suski, K. J., Hill, T. C. J., Levin, E. J. T., Miller, A., DeMott, P. J., & Kreidenweis, S. M. (2018). Agricultural harvesting emissions of ice-nucleating particles. *Atmospheric Chemistry and Physics*, *18*(18), 13,755–13,771. https://doi.org/10.5194/acp-18-13755-2018

Swain, D. L., Langenbrunner, B., Neelin, J. D., & Hall, A. (2018). Increasing precipitation volatility in twenty-first-century California. *Nature Climate Change*, *8*(5), 427–433. https://doi.org/10.1038/s41558-018-0140-y

Tobo, Y., Prenni, A. J., DeMott, P. J., Huffman, J. A., McCluskey, C. S., Tian, G. X., et al. (2013). Biological aerosol particles as a key determinant of ice nuclei populations in a forest ecosystem. *Journal of Geophysical Research: Atmospheres*, *118*, 10100–10110. https://doi.org/10.1002/jgrd.50801

Ullrich, R., Hoose, C., Mohler, O., Niemand, M., Wagner, R., Hohler, K., et al. (2017). A New Ice Nucleation Active Site Parameterization for Desert Dust and Soot. *Journal of the Atmospheric Sciences*, *74*(3), 699–717. https://doi.org/10.1175/jas-d-16-0074.1

Vali, G. (1971). Supercooling of Water and Nucleation of Ice (Drop Freezer). *American Journal of Physics*, 1125–&. *19*(7). https://doi.org/10.1119/1.1976585 Vali, G., DeMott, P. J., Mohler, O., & Whale, T. F. (2015). Technical Note: A proposal for ice nucleation terminology. *Atmospheric Chemistry and Physics*, *15*(18), 10,263–10,270. https://doi.org/10.5194/acp-15-10263-2015

Wright, T. P., Hader, J. D., McMeeking, G. R., & Petters, M. D. (2014). High Relative Humidity as a Trigger for Widespread Release of Ice Nuclei. *Aerosol Science and Technology*, *48*(11). https://doi.org/10.1080/02786826.2014.968244